

**Attitude Synchronization of Spacecraft Formation with Optimization and  
Adaptation of Consensus Penalty Terms**

by

Kewen Zhang

A Thesis

Submitted to the Faculty

of the

WORCESTER POLYTECHNIC INSTITUTE

in partial fulfillment of the requirements for the

Degree of Master of Science

in

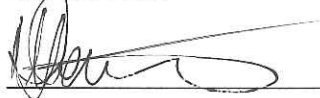
Mechanical Engineering

by



April 2013

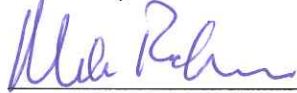
APPROVED:



Dr. Michael A. Demetriou, Advisor  
Professor, Mechanical Engineering Department



Dr. Nikolaos A. Gatsonis, Committee Member  
Professor, Mechanical Engineering Department



Dr. Mark W. Richman, Committee Member  
Associate Professor, Mechanical Engineering Department



Dr. Simon W. Evans, Graduate Committee Representative  
Assistant Professor, Mechanical Engineering Department

# Abstract

The contribution of this thesis is on the temporal adjustment of the consensus weights, as applied to spacecraft formation control. Such an objective is attained by dynamically enforcing attitude synchronization via coupling terms included in each spacecraft controller. It is assumed that each spacecraft has identical dynamics but with unknown inertia parameters and external disturbances. By augmenting a standard adaptive controller that accounts for the unknown parameters, made feasible via an assumption on parameterization, with adaptation of the consensus weights, one opts to improve spacecraft synchronization. The coupling terms, responsible for enforcing synchronization amongst spacecraft, are weighted dynamically in proportion to the disagreement between the states of the spacecraft. The time adjustment of edge-dependent gains as well as the special cases of node-dependent and agent-independent constant gains are derived using Lyapunov redesign methods. The proposed adaptive control architectures which allow for adaptation of both parameter uncertainties and consensus penalty terms are demonstrated via extensive numerical studies of spacecraft networks with limited connectivity. By considering the sum of deviation-from-the-mean and rotational kinetic energy as appropriate metrics for synchronization and controller performance, the numerical studies also provide insights on the choice of optimal consensus gains.

# Acknowledgements

I would like to express my appreciation to my advisor Dr. Michael A. Demetriou. Thanks for his time, patience, responsibility and understanding. It has been an honor to work with you. I would like to also thank Professors Gatsonis, Richman and Evans for their willingness to serve in my thesis committee.

My gratitude also goes to my parents. You give me your unconditional support and love through all my way for pursuing my dream. There are not enough words to describe my love to you.

# Table of Contents

<b>Abstract</b>	<b>i</b>
<b>Acknowledgements</b>	<b>ii</b>
<b>Table of Contents</b>	<b>iii</b>
<b>List of Figures</b>	<b>v</b>
<b>List of Tables</b>	<b>vii</b>
<b>1 Introduction</b>	<b>1</b>
1.1 Motivation and Related Work.....	1
1.2 Thesis Objectives .....	4
1.3 Thesis Organization .....	5
<b>2 Problem Formulation and Background</b>	<b>7</b>
2.1 Lagrangian Formulation.....	7
2.2 Attitude Dynamics .....	8
2.3 Graph theory .....	11
2.4 Barbălat’ s Lemma .....	14
<b>3 Attitude Synchronization of Spacecraft Formation with Known Parameters</b>	<b>15</b>
3.1 Edge-dependent fixed synchronization gains .....	16
3.2 Adaptation of synchronization penalty terms for Edge-dependent gains .....	19
<b>4 Attitude Synchronization of Spacecraft Formation with Unknown Parameters</b>	<b>23</b>
4.1 Edge-dependent fixed synchronization gains for parameter uncertainty case .....	23
4.2 Edge-dependent time-varying gains for the parameter uncertainty case .....	26
<b>5 Numerical Simulation</b>	<b>29</b>
5.1 Numerical study for the case of known parameters .....	30
5.1.1 Effect of constant synchronization gains on system performance .....	32
5.1.2 Effect of adaptation of synchronization gains .....	36
5.2 Numerical study for the case of unknown parameters .....	40
5.3 Example of more complex communication topology .....	45
5.3.1 Communication topology with directed graph .....	45
5.3.2 Communication topology with undirected graph .....	50
5.4 Specific study on the effect of adaptation of synchronization gains .....	55

<b>6 Conclusion and Future Work</b>	<b>59</b>
6.1 Conclusion .....	59
6.2 Future work.....	60
<b>References</b>	<b>61</b>

# List of Figures

Figure 1: A graph on 4 vertices. ....	12
Figure 2: A digraph on 4 vertices. ....	13
Figure 3: Section 5.1 Directed graph on 4 spacecraft.....	31
Figure 4: Section 5.1.1 Evolution of attitude error with constant edge-dependent gain.....	33
Figure 5: Section 5.1.1 Evolution of angular velocity with constant edge-dependent gain.....	34
Figure 6: Section 5.1.1 Evolution of $\sqrt{\ \Delta(t)\ ^2 + E_r^2(t)}$ .....	35
Figure 7: Section 5.1.1 The effects of varying the uniform fixed gain in the range $0 < \mu \leq 6$ on $\ \Delta(t)\ $ and $E_r(t)$ .....	36
Figure 8: Section 5.1.2 Evolution of attitude error with adaptive edge-dependent gain.....	37
Figure 9: Section 5.1.2 Evolution of angular velocity with adaptive edge-dependent gain.....	38
Figure 10: Section 5.1.2 Evolution of $\sqrt{\ \Delta(t)\ ^2 + E_r^2(t)}$ .....	39
Figure 11: Section 5.1.2 The effects of adaptive edge-dependent gain on $\ \Delta(t)\ $ and $E_r(t)$ in the range $0.1 \leq \alpha \leq 2.1$ . ....	40
Figure 12: Section 5.2 Evolution of attitude error with constant edge-dependent gain.....	41
Figure 13: Section 5.2 Evolution of angular velocity with constant edge-dependent gain.....	42
Figure 14: Section 5.2 The effects of constant edge-dependent gain on $\ \Delta(t)\ $ and $E_r(t)$ in the range $0.1 \leq \alpha \leq 2$ .....	43
Figure 15: Section 5.2 Evolution of attitude error with adaptive edge-dependent gain.....	44
Figure 16: Section 5.2 Evolution of angular velocity with adaptive edge-dependent gain.....	45
Figure 17: Section 5.3.1 Directed graph on 7 spacecraft.....	46
Figure 18: Section 5.3.1 Evolution of attitude error with constant edge-dependent gain.....	47
Figure 19: Section 5.3.1 Evolution of angular velocity with constant edge-dependent gain.....	48

<b>Figure 20: Section 5.3.1 The effects of varying the uniform fixed gain in the range <math>0.5 \leq \mu \leq 6</math> on <math>\ \Delta(t)\ </math> and <math>E_r(t)</math>.</b>	<b>49</b>
<b>Figure 21: Section 5.3.1 The effects of adaptive edge-dependent gain on <math>\ \Delta(t)\ </math> and <math>E_r(t)</math> in the range <math>0.5 \leq \alpha \leq 6</math>.</b>	<b>50</b>
<b>Figure 22: Section 5.3.2 Undirected graph on 7 spacecraft.</b>	<b>51</b>
<b>Figure 23: Section 5.3.2 Evolution of attitude error with constant edge-dependent gain.</b>	<b>52</b>
<b>Figure 24: Section 5.3.2 Evolution of angular velocity with constant edge-dependent gain.</b>	<b>53</b>
<b>Figure 25: Section 5.3.2 The effects of varying the uniform fixed gain on the range <math>0.1 \leq \mu \leq 6</math> on <math>\ \Delta(t)\ </math> and <math>E_r(t)</math>.</b>	<b>54</b>
<b>Figure 26: Section 5.3.2 The effects of edge-dependent gain on <math>\ \Delta(t)\ </math> and <math>E_r(t)</math> in the range <math>0.3 \leq \alpha \leq 6</math>.</b>	<b>55</b>
<b>Figure 27: Section 5.4 Communication topology with 2 spacecraft.</b>	<b>56</b>
<b>Figure 28: Section 5.4 The effects of adaptive edge-dependent gain on <math>\ \Delta(t)\ </math> and <math>E_r(t)</math> with different <math>\lambda_{12}^*</math> and <math>\lambda_{21}^*</math>.</b>	<b>57</b>

# List of Tables

**Table 1:  $L_2(0, 10)$  norm of  $\|\Delta(t)\|^2 + E_T^2(t)$  ..... 58**

# Chapter 1

## Introduction

### 1.1 Motivation and Related Work

The application of synchronization control provides remarkable advantages in solving problems associated with multi-agent systems and in particular spacecraft formation. In space industry, coordination capabilities of multi-agent systems involve sensing, communicating and synchronizing the motion [1]. Any additional improvements in control algorithms would translate to significant energy savings. One such improvement involves optimization and adjustment of consensus gains as used for synchronization control of spacecraft formation.

Spacecraft formation aims to force multiple spacecraft to work together in a group, while maintaining certain coordinated attitude dynamics. Such group behavior has many benefits over single satellites including great flexibility, reduced cost, overall adaptability and simple design. The optimization and adjustment of consensus gains for improving the attitude synchronization has attracted vast of interests in the past years.

References [2] and [3] provide a comprehensive survey of spacecraft formation flying guidance and control.

The current effort continues on the earlier works. A set of adaptive strategies for synchronization of complex networks is proposed in [4] where the adaptation law is based on the information at the network nodes. Reference [5] analyzed the synchronization of networked nonlinear oscillator, using the time varying local gains. In [6], a decentralized strategy for synchronization is presented based on adaptive local gains, which is robust to topological variation and time-delay. Although these works considered the adaptation of gains involving the pairwise mismatch of the orientation states, generally the strategy they used to guarantee the attitude synchronization of spacecraft formation imposed conservative conditions.

In [7], the authors developed a passivity-based distributed velocity input law to investigate attitude synchronization in the Special Euclidean group, with the assumption that information exchange among the agents are under strongly connected. It also showed that the control input is suitable for the leader-follower case and the cases with communication delay and topology switching. The work in [8] considered attitude synchronization for a group of spacecraft in the presence of attitude forbidden zones. It introduced the quadratic convex parameterization to find a feasible consensus like algorithm, and embed it into an auxiliary system which utilizes a logarithmic barrier potential to measure the attitude deviation from the boundary of the constrained zone. With the information from the auxiliary system and neighbor spacecraft, attitude synchronization can be achieved.

In practical cases, the true value of parameters is hard to determine exactly. A way to address parametric uncertainties and external disturbances, as for example externally generated environmental torques, is to employ adaptive control methods. Beyond stabilizability and tracking or regulation, which can be ensured by implementing robust or adaptive controllers, the attitude synchronization problem requires additional control design. This comes in the form of additive consensus terms in the controllers and consists of terms that penalize the mismatch between the spacecraft states. For example, the penalty terms in each spacecraft controller may include the pairwise difference of spacecraft angular velocities, weighted by appropriately chosen penalty gains. Continuing with possible improvements of the consensus terms used for spacecraft synchronization, is the temporal adjustment of the consensus gains. When the “disagreement” of spacecraft  $i$  with spacecraft  $j$  is “smaller” than the disagreement of spacecraft  $i$  with spacecraft  $k$ , then the gain of the first disagreement should be less than that of the second pairwise difference. This would then allow for significant reductions in controller magnitudes and provide additional robustness due to uncertainties.

In [9], an adaptive controller was established based on Lyapunov theory. It entailed control theory for delay-free and coupling time-delay topologies to achieve attitude synchronization of spacecraft formation. The control architecture introduced allowed for parameter uncertainties. The plant parameters were parameterized via a suitable transformation and the control signal consisted of two parts: (1) the regulation or model following part coupled with adaptation of plant parameters and (2) the part that enforced consensus. The latter involved coupling gains of pairwise differences of the spacecraft states. Such penalization involved gains that were constant and uniform with

respect to the  $N$  agents. Both the static regulation and the dynamic tracking cases were analyzed. The work in [10] addressed the cooperative tracking problem in the presence of model uncertainties and time-varying delay, especially the development of an output feedback control law without explicitly requiring the information of angular velocity. [11] proposed adaptive schemes for unknown parameters in system dynamics in the way of coordinating torques and control laws by position and velocity errors. [12] considered the problem of bilateral teleoperation with unknown parameters and developed a passive coordination control to synchronize the states of master and slave robots.

The framework considered in this work for the attitude synchronization is based on the dynamic framework in Lagrangian form, which is convenient when dealing with multiple systems. The application of Lagrangian formulation for dynamic model in Robotics is widely used [13]. For example, [11], [12] propose adaptive coordination architectures to ensure synchronization in both positions and velocities for teleoperators with time-delay. The stability analysis and controller synthesis used is similar to the case of spacecraft formation. For example, [14] studies synchronization for both translational and rotational dynamics in the Lagrangian form using contraction analysis.

## **1.2 Thesis Contributions**

In this thesis, the attitude synchronization of spacecraft formation is considered and in particular the optimization and time adaptation of the consensus weights used for synchronization. This work extends the work of [9] with the difference that it adapts the consensus (local) weights in the control signal. Extending the case of uniformly fixed-gains in the synchronization signal, three types of consensus gains are considered: (i)

**node-dependent** (the local weights of the synchronization signal can differ for each spacecraft) (ii) **constant gain, edge-dependent** (the local weights can differ for each spacecraft and for each of its communication neighbors) constant gain and (iii) **time-varying edge-dependent gains**. The case of adaptive adjustment of the gains leads to combined control and adaptation laws. The proposed modification assumes that the synchronization signal contains a fixed gain but the torque inputs are weighted by a local adaptive gain. Using Lyapunov redesign methods, the adaptation laws for the local gains are derived and the synchronization objective can subsequently be established. Furthermore, the main contribution of this work also includes the time-adjustment of the unknown parameters of the system dynamics when consider the practical case of parameter uncertainty. Additionally, this work also provides insights on the choice of optimal consensus gains considering keeping a low cost of energy.

### 1.3 Thesis Organization

In Chapter 2, the formulation of the problem is presented as well as the background on the attitude dynamics and graph theory. Firstly, the synchronizing controllers for known parameters are presented in Chapter 3. This chapter mainly considers edge-dependent synchronization gains which includes the special cases of node-dependent and uniform weights, as well as the adaptive adjustment of the edge-dependent synchronization gains. Their applications for the cases of parameter uncertainty are provided in Chapter 4. The stability analysis and convergence properties of the proposed control architectures are presented in both Chapter 3 and 4.

In Chapter 5, numerical studies on the effects of the synchronization gains on both a measure of agreement of the spacecraft states and on the rotational kinetic energy are presented. Conclusions and Future work follow in Chapter 6.

# Chapter 2

## Problem Formulation and Background

In this chapter, the dynamic model based on the Euler-Lagrange formulation for the networked spacecraft system is established. Additionally, it provides background for the graph theory used in communication topology.

### 2.1 Lagrangian Formulation

The natural form of the Lagrangian is defined as the total kinetic energy  $T$  minus the potential energy  $U$

$$L = T - U$$

where the kinetic energy is given by

$$T = \frac{1}{2} \dot{\mathbf{q}}^T \mathbf{M} \dot{\mathbf{q}}$$

where  $\mathbf{M}$  is the inertial matrix. Then the equation of motion of the system can be achieved in the expression of the Euler-Lagrange equation. That is, the dynamic equation of motion can be described as

$$\frac{d}{dt} \frac{\partial L}{\partial \dot{\mathbf{q}}} - \frac{\partial L}{\partial \mathbf{q}} = \boldsymbol{\tau}$$

where  $\mathbf{q} \in \mathbb{R}^n$  is the generalized coordinate with multiple degrees of freedom  $n$ ,  $\boldsymbol{\tau}$  is the external force.

The above equation can be written in the form of [13]

$$\mathbf{M}(\mathbf{q})\ddot{\mathbf{q}} + \mathbf{C}(\mathbf{q}, \dot{\mathbf{q}})\dot{\mathbf{q}} + \boldsymbol{\tau}_g(\mathbf{q}) = \boldsymbol{\tau}$$

where  $\mathbf{M}$  is an  $n \times n$  symmetric, positive-definite inertia matrix,  $\mathbf{C}$  is an  $n \times n$  matrix and  $\mathbf{C}\dot{\mathbf{q}}$  is the vector of Coriolis and centrifugal terms, and  $\boldsymbol{\tau}_g$  is the vector of gravity terms. Here  $\mathbf{C}$  is defined using the Christoffel symbols of the first type and given by [13].

## 2.2 Attitude Dynamics

A group of  $N$  networked spacecraft having identical dynamics is considered. Using the Euler rotational equations of motion, one can arrive at the following equations that describe the dynamics for each spacecraft in body axes

$$\mathbf{J}\dot{\boldsymbol{\omega}} - (\mathbf{J}\boldsymbol{\omega}) \times \boldsymbol{\omega} = \mathbf{u} + \mathbf{d}_{\text{ext}}$$

where  $\mathbf{J}$  is the total inertia matrix and  $\boldsymbol{\omega}$  is the angular velocity vector. The input signals  $\mathbf{u}$  and  $\mathbf{d}_{\text{ext}} \in \mathbb{R}^3$  denote the control and external disturbance torques respectively. All these parameters are described in the body frame.

In this thesis, the orientation of spacecraft with respect to the inertial frame will be expressed in the way of Modified Rodrigues Parameters (MRP) [15] [16] [17]. The

advantages of the use of MRPs include: there is no additional equality constraint as for the quaternion case; they can parameterize eigenaxis rotations up to 360 degrees and provide a continuous single-valued and analytic representation of rotations [16]. In this way, the attitude vector  $\mathbf{q} \in \mathbb{R}^3$  should be  $\mathbf{q}(\hat{\mathbf{n}}, \theta) = \tan\left(\frac{\theta}{4}\right) \hat{\mathbf{n}}$ , where  $\hat{\mathbf{n}}$  is the eigenaxis unit vector and  $-2\pi < \theta < 2\pi$  is the eigenangle. Therefore, the attitude vector  $\mathbf{q}$  and the angular velocity  $\boldsymbol{\omega}$  have the following relationship

$$\dot{\mathbf{q}} = \mathbf{Z}(\mathbf{q})\boldsymbol{\omega} \quad (1)$$

where

$$\mathbf{Z}(\mathbf{q}) = \frac{1}{2} \left( \frac{1}{2} (1 - \mathbf{q}^T \mathbf{q}) \mathbf{I}_3 + \mathbf{q} \mathbf{q}^T + \mathbf{S}(\mathbf{q}) \right)$$

and the skew-symmetric matrix  $\mathbf{S}(\mathbf{q})$  is defined as

$$\mathbf{S}(\mathbf{q}) = \begin{bmatrix} 0 & -q_3 & q_1 \\ q_3 & 0 & q_2 \\ -q_2 & -q_1 & 0 \end{bmatrix}$$

In matrix notation, the rotational kinetic energy of a rigid body is written as [18]

$$T = \frac{1}{2} \boldsymbol{\omega}^T \mathbf{H} = \frac{1}{2} \boldsymbol{\omega}^T \mathbf{J} \boldsymbol{\omega}$$

where  $\mathbf{H} = \mathbf{J} \boldsymbol{\omega}$  is the angular momentum.

Using the notation of MRP to get

$$T = \frac{1}{2} \boldsymbol{\omega}^T \mathbf{J} \boldsymbol{\omega} = \frac{1}{2} \dot{\mathbf{q}}^T \mathbf{Z}^{-T} \mathbf{J} \mathbf{Z}^{-1} \dot{\mathbf{q}} = \frac{1}{2} \dot{\mathbf{q}}^T \mathbf{M} \dot{\mathbf{q}},$$

$$L = T - U = \frac{1}{2} \dot{\mathbf{q}}^T \mathbf{M} \dot{\mathbf{q}} - U(\mathbf{q})$$

where  $\mathbf{M}(\mathbf{q}) = \mathbf{Z}^{-T}(\mathbf{q}) \mathbf{J} \mathbf{Z}^{-1}(\mathbf{q})$  is the inertial matrix. According to the Euler-Lagrangian equation

$$\frac{d}{dt} \frac{\partial L}{\partial \dot{\mathbf{q}}} - \frac{\partial L}{\partial \mathbf{q}} = \boldsymbol{\tau}$$

$$\frac{d}{dt} \frac{\partial L}{\partial \dot{\mathbf{q}}} = \frac{d}{dt} (\mathbf{M}\dot{\mathbf{q}}) = \dot{\mathbf{M}}\dot{\mathbf{q}} + \mathbf{M}\ddot{\mathbf{q}}$$

$$\frac{\partial L}{\partial \mathbf{q}} = \frac{1}{2} \dot{\mathbf{q}}^T \frac{\partial \mathbf{M}}{\partial \mathbf{q}} \dot{\mathbf{q}} + \frac{dU(\mathbf{q})}{d\mathbf{q}}$$

$$\frac{d}{dt} \frac{\partial L}{\partial \dot{\mathbf{q}}} - \frac{\partial L}{\partial \mathbf{q}} = \mathbf{M}\ddot{\mathbf{q}} + \dot{\mathbf{M}}\dot{\mathbf{q}} - \frac{1}{2} \dot{\mathbf{q}}^T \frac{\partial \mathbf{M}}{\partial \mathbf{q}} \dot{\mathbf{q}} + \frac{dU(\mathbf{q})}{d\mathbf{q}}$$

One can express the attitude dynamics through Euler-Lagrange formulation [14]

$$\dot{\mathbf{M}}\dot{\mathbf{q}} - \frac{1}{2} \dot{\mathbf{q}}^T \frac{\partial \mathbf{M}}{\partial \mathbf{q}} \dot{\mathbf{q}} = \frac{\partial \mathbf{M}}{\partial \mathbf{q}} \dot{\mathbf{q}}\dot{\mathbf{q}} - \frac{1}{2} \dot{\mathbf{q}}^T \frac{\partial \mathbf{M}}{\partial \mathbf{q}} \dot{\mathbf{q}} = \left( \frac{\partial \mathbf{M}}{\partial \mathbf{q}} \dot{\mathbf{q}} - \frac{1}{2} \dot{\mathbf{q}}^T \frac{\partial \mathbf{M}}{\partial \mathbf{q}} \right) \dot{\mathbf{q}} = \mathbf{C}(\mathbf{q}_i, \dot{\mathbf{q}}_i) \dot{\mathbf{q}}_i$$

The  $\mathbf{C}$  matrix is defined as

$$c_{ij} = \frac{1}{2} \sum_{k=1}^n \frac{\partial M_{ij}}{\partial q_k} \dot{q}_k + \frac{1}{2} \sum_{k=1}^n \left( \frac{\partial M_{ik}}{\partial q_j} - \frac{\partial M_{jk}}{\partial q_i} \right) \dot{q}_k$$

$$\frac{dU(\mathbf{q})}{d\mathbf{q}} = \boldsymbol{\tau}_{ext,i}$$

Therefore, for every individual spacecraft, the attitude dynamics can be expressed as

$$\mathbf{M}_i(\mathbf{q}_i) \ddot{\mathbf{q}}_i + \mathbf{C}_i(\mathbf{q}_i, \dot{\mathbf{q}}_i) \dot{\mathbf{q}}_i = \boldsymbol{\tau}_i + \boldsymbol{\tau}_{ext,i} \quad (2)$$

where index  $i \in \{1, 2, \dots, N\}$  is the set of networked spacecraft, and

$$\mathbf{M}_i(\mathbf{q}_i) = \mathbf{Z}^{-T}(\mathbf{q}_i) \mathbf{J}_i \mathbf{Z}^{-1}(\mathbf{q}_i)$$

$$\mathbf{C}_i(\mathbf{q}_i, \dot{\mathbf{q}}_i) = -\mathbf{Z}^{-T}(\mathbf{q}_i) \mathbf{J}_i \dot{\mathbf{Z}}(\mathbf{q}_i) \mathbf{Z}^{-1}(\mathbf{q}_i) - \mathbf{Z}^{-T}(\mathbf{q}_i) \mathbf{S}(\mathbf{J}_i \boldsymbol{\omega}_i) \mathbf{Z}^{-1}(\mathbf{q}_i)$$

$$\boldsymbol{\tau}_i = \mathbf{Z}^{-T}(\mathbf{q}_i) \mathbf{u}_i$$

$$\boldsymbol{\tau}_{ext,i} = \mathbf{Z}^{-T}(\mathbf{q}_i) \mathbf{d}_{ext,i}$$

The above dynamical equation is linear in the parameters as long as  $\mathbf{d}_{ext}$  is constant. The

above Euler-Lagrange formulation enjoys some fundamental properties, summarized

below [1], [13], [19], [20], [21].

**Property 1:** The inertia matrix  $\mathbf{M}_i(\mathbf{q}_i)$  is lower and upper bounded, *i.e.* for each  $i = 1, \dots, N$

$$0 < \lambda_m\{\mathbf{M}_i\}I \leq \mathbf{M}_i(\mathbf{q}_i) \leq \lambda_M\{\mathbf{M}_i\}I < \infty$$

**Property 2:** The matrix  $(\dot{\mathbf{M}}_i(\mathbf{q}_i) - 2\mathbf{C}_i(\mathbf{q}_i, \dot{\mathbf{q}}_i))$  is skew-symmetric, that is for any vector  $\mathbf{v} \in \mathbb{R}^3$

$$\mathbf{v}^T (\dot{\mathbf{M}}_i(\mathbf{q}_i) - 2\mathbf{C}_i(\mathbf{q}_i, \dot{\mathbf{q}}_i)) \mathbf{v} = 0$$

**Property 3:** The Coriolis term  $\mathbf{C}_i(\mathbf{q}_i, \dot{\mathbf{q}}_i)$  is bounded as  $\forall \mathbf{q}_i, \dot{\mathbf{q}}_i, \exists k > 0 \in \mathbb{R}$

$$|\mathbf{C}_i(\mathbf{q}_i, \dot{\mathbf{q}}_i)\dot{\mathbf{q}}_i| \leq k|\dot{\mathbf{q}}_i|^2$$

**Property 4:** With constant  $\mathbf{d}_{ext}$  and inertial moments, (2) is linearly parameterizable, *i.e.* it admits the expansion

$$\mathbf{M}_i(\mathbf{q}_i)\ddot{\mathbf{q}}_i + \mathbf{C}_i(\mathbf{q}_i, \dot{\mathbf{q}}_i)\dot{\mathbf{q}}_i - \boldsymbol{\tau}_{ext,i} = \mathbf{Y}(\mathbf{q}_i, \dot{\mathbf{q}}_i, \ddot{\mathbf{q}}_i)\boldsymbol{\theta}_i = \boldsymbol{\tau}_i(t)$$

where  $\boldsymbol{\theta}_i$  is a constant  $p$ -dimensional vector of parameters whose elements include the moments of inertial and external disturbances, and  $\mathbf{Y}(\mathbf{q}_i, \dot{\mathbf{q}}_i, \ddot{\mathbf{q}}_i) \in \mathbb{R}^{p \times p}$  is the matrix of known functions depending on the generalized coordinates and their higher derivatives.

### 2.3 Graph theory

The graph theoretic framework provides means to examine the correspondence of the networked systems. The algebraic attributes of the network topology pave the way to analyze and synthesize the networked dynamic systems. Formally, a graph [22] shown in Figure 1 is defined as the pair  $\mathcal{G} = (V, E)$ , where  $V$  denotes the set of vertices  $\{v_1, v_2, \dots, v_N\}$ ,  $E \subseteq V \times V$  denotes the set of edges. The set of neighbors of a given agent (spacecraft) is denoted by  $N_i$ ,  $i = 1, \dots, N$ .

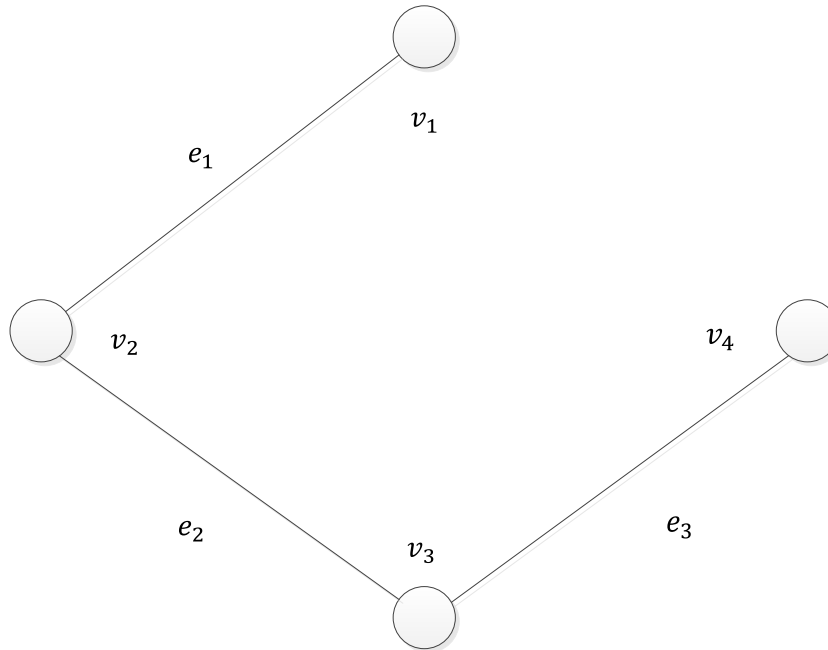


**Figure 1: A graph on 4 vertices.**

If for every pair of vertices, there is a path that has them as its end vertices, the graph is connected. When the vertices of the path are distinct except for its end vertices, the path is called a cycle [22].

A graph containing no cycles is called a forest. When it is connected, this forest is called a tree. If the tree spans all over the graph, it becomes a spanning tree [23].

When the communication between the networked system has certain directions, a directed graph can be constructed (see Figure 2). In digraph, if the ordered pair  $v_i v_j \in E$ , this means edge  $v_i v_j$  is to originate in  $v_i$  and terminate in  $v_j$ .

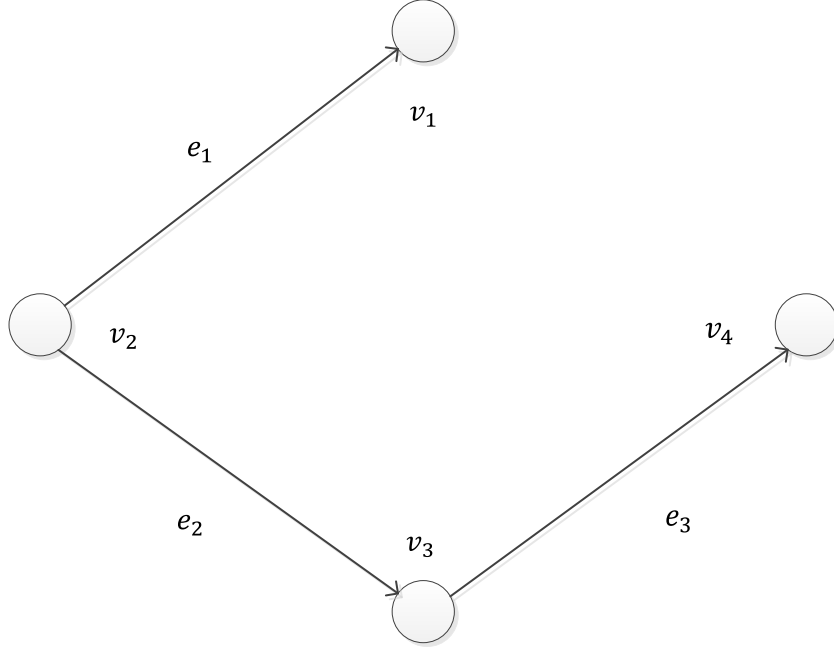


**Figure 2: A digraph on 4 vertices.**

According to Definition 2.11 in [22], there is an important notation for a digraph. A digraph is a rooted out-branching if it does not contain a directed cycle and it has a vertex  $v_r$  (the root) such that for every other vertex there is a directed path from  $v_r$  to  $v$ .

The adjacency matrix  $A(\mathcal{G})$  is the symmetric  $n \times n$  matrix, where  $[A(\mathcal{G})]_{ij} = 1$  if edge  $v_i v_j \in E$ , otherwise  $[A(\mathcal{G})]_{ij} = 0$ . The degree of a given vertex is equal to the number of vertices that are adjacent to the vertex  $v_i$  in  $\mathcal{G}$ . An important notation is the graph Laplacian of  $\mathcal{G}$  which is defined as  $L(\mathcal{G}) = \Delta(\mathcal{G}) - A(\mathcal{G})$ , where  $\Delta(\mathcal{G})$  is the degree matrix of  $\mathcal{G}$ . For example, the Laplacian matrix of the graph in Figure 1 is

$$L(\mathcal{G}) = \begin{bmatrix} 1 & -1 & 0 & 0 \\ -1 & 2 & -1 & 0 \\ 0 & -1 & 2 & -1 \\ 0 & 0 & -1 & 1 \end{bmatrix}$$

and the Laplacian matrix of the digraph in Figure 2 is

$$L(\mathcal{G}) = \begin{bmatrix} 1 & -1 & 0 & 0 \\ 0 & 0 & 0 & 0 \\ 0 & -1 & 1 & 0 \\ 0 & 0 & -1 & 1 \end{bmatrix}$$

According to Theorem 2.8 and Theorem 3.4 in [22], the graph Laplacian of a connected graph has one 0 eigenvalue and others have positive real part. And the agreement protocol converges the agreement set with a rate of convergence that is dictated by the second minimal eigenvalue. Similarly, a directed agreement protocol will converge to an agreement set as long as the digraph contains a rooted out-branching. Besides, a digraph containing a rooted out-branching as a subgraph has  $\text{rank } L(\mathcal{G}) = n - 1$ , and  $N(L(\mathcal{G}))$  is spanned by the vector of all ones.

In this work, the underlying interaction topology among the spacecraft has the following assumption.

**Assumption 1:** The communication graph is fixed and connected or the digraph has rooted out-branching.

## 2.4 Barbălat's Lemma

Usually it is hard to examine the asymptotic stability analysis of time-varying systems, since it is difficult to find Lyapunov functions with a negative definite derivative. Barbălat's lemma is a very important result when one deals with this situation [24].

**Lemma 1:** If the differentiable function  $f(t)$  has a finite limit as  $t \rightarrow \infty$ , and if  $\dot{f}$  is uniformly continuous, then  $\dot{f}(t) \rightarrow 0$  as  $t \rightarrow \infty$ .

## Chapter 3

# Attitude Synchronization of Spacecraft Formation with Known Parameters

One way to improve the performance of synchronizing controllers, short of considering time variation via adaptive adjustment, is to consider different synchronization gains for each agent. Such a case is called *node-dependent synchronization gain* case, *i.e.* each agent will have a different synchronization gain from the other agents. Going further, one may consider having different gains for each pairwise difference between the state of an agent and the states of its neighboring agents. This is the *edge-dependent synchronization gain* case [25]. This modification has additional flexibility compared to the node-dependent gain case; the latter is in fact a special case of the edge-dependent gain, which will be proved in the following content.

In Section 3.1, the synchronizing controllers with edge-dependent constant weights are presented and their time adaptation is given in Section 3.2. In the following treatment, both the inertial parameters and external disturbance are assumed to be known.

In this work, only regulation is considered. Thus the following conditions, which constitute the synchronization objectives, should be satisfied

$$\begin{aligned} \lim_{t \rightarrow \infty} |\mathbf{q}_i - \mathbf{q}_j| &= 0 \\ \lim_{t \rightarrow \infty} |\boldsymbol{\omega}_i| &= 0 \end{aligned} \quad i = 1, \dots, N, j \in N_i. \quad (3)$$

### 3.1 Edge-dependent fixed synchronization gains

Using the edge-dependent modification, the synchronization signal of the  $i$ -th spacecraft is now given by [25]

$$\mathbf{w}_i(t) \triangleq \dot{\mathbf{q}}_i(t) + \sum_{j \in N_i} \mu_{ij} (\mathbf{q}_i(t) - \mathbf{q}_j(t)) \quad (4)$$

where  $\mu_{ij} > 0$  is the edge-dependent gain and  $N_i$  denotes the neighbors of node  $i$ .

From the above equation, one can observe that the pairwise differences between the state of the  $i$ -th spacecraft and the state of its neighbor  $j$ ,  $j \in N_i$  are varying with both  $i$  and  $j$ .

For notational simplification, define the error between the  $i$ -th spacecraft and its neighbor

$$\mathbf{q}_{ij}(t) = \mathbf{q}_i(t) - \mathbf{q}_j(t), \quad i = 1, \dots, N, j \in N_i$$

Then, for the attitude dynamics (3), use the following control law

$$\boldsymbol{\tau}_i = -\sum_{j \in N_i} \mu_{ij} (\mathbf{M}_i \dot{\mathbf{q}}_{ij} + \mathbf{C}_i \mathbf{q}_{ij}) - \boldsymbol{\tau}_{ext,i} + \bar{\boldsymbol{\tau}}_i \quad (5)$$

With the proposed control law equation (5), the closed-loop system is now given by

$$\mathbf{M}_i(q_i) \ddot{\mathbf{q}}_i + \mathbf{C}_i(q_i, \dot{\mathbf{q}}_i) \dot{\mathbf{q}}_i = -\sum_{j \in N_i} \mu_{ij} (\mathbf{M}_i \dot{\mathbf{q}}_{ij} + \mathbf{C}_i \mathbf{q}_{ij}) + \bar{\boldsymbol{\tau}}_i \quad (6)$$

Now, using the definition of the synchronization signal equation (4), one can express the closed loop system equation (6) in terms of the synchronization signal  $\mathbf{w}_i$

$$\mathbf{M}_i \left( \dot{\mathbf{w}}_i - \sum_{j \in N_i} \mu_{ij} \dot{\mathbf{q}}_{ij} \right) + \mathbf{C}_i \left( \mathbf{w}_i - \sum_{j \in N_i} \mu_{ij} \mathbf{q}_{ij} \right) = - \sum_{j \in N_i} \mu_{ij} (\mathbf{M}_i \dot{\mathbf{q}}_{ij} + \mathbf{C}_i \mathbf{q}_{ij}) + \bar{\boldsymbol{\tau}}_i$$

or

$$\mathbf{M}_i \dot{\mathbf{w}}_i + \mathbf{C}_i \mathbf{w}_i = \bar{\boldsymbol{\tau}}_i \quad (7)$$

**Theorem 1:** With Assumption 1 and control architecture (7), the attitude synchronization objective in the sense of (3) is attained by choosing  $\bar{\boldsymbol{\tau}}_i = -\mathbf{K}_i \mathbf{w}_i$ , where  $\mathbf{K}_i$  is a symmetric positive definite matrix.

*Proof:* Construct a Lyapunov function

$$V_i = \frac{1}{2} \mathbf{w}_i^T \mathbf{M}_i \mathbf{w}_i, \quad i = 1, \dots, N$$

Using property (P2) and the control law  $\bar{\boldsymbol{\tau}}_i = -\mathbf{K}_i \mathbf{w}_i$ , the derivative of  $V_i$  along the trajectories of equation (7) is given by

$$\begin{aligned} \dot{V}_i &= \frac{1}{2} \mathbf{w}_i^T \dot{\mathbf{M}}_i \mathbf{w}_i + \mathbf{w}_i^T \mathbf{M}_i \dot{\mathbf{w}}_i = \frac{1}{2} \mathbf{w}_i^T (\dot{\mathbf{M}}_i - 2\mathbf{C}_i + 2\mathbf{C}_i) \mathbf{w}_i + \mathbf{w}_i^T (\bar{\boldsymbol{\tau}}_i - \mathbf{C}_i \mathbf{w}_i) \\ &= \mathbf{w}_i^T \bar{\boldsymbol{\tau}}_i = -\mathbf{w}_i^T \mathbf{K}_i \mathbf{w}_i < 0 \end{aligned}$$

Since  $\mathbf{M}_i$  is bounded (property (P1)) and  $\mathbf{K}_i$  is a positive-definite design matrix, then  $V_i$  is bounded with  $\dot{V}_i < -\alpha \mathbf{w}_i^T \mathbf{K}_i \mathbf{w}_i$ , where  $\alpha = \lambda_{\min}(\mathbf{K}_i)$  is a positive constant. A consequence of Lyapunov stability theorem [26] is that  $\mathbf{w}_i \in \mathcal{L}_\infty$  and  $\lim_{t \rightarrow \infty} |\mathbf{w}_i| = 0$ . In fact, the convergence is exponential! Now, rewrite equation (4) as

$$\mathbf{w}(t) = \dot{\mathbf{q}} + (\mathbf{L}^* \otimes \mathbf{I}_3) \mathbf{q} \quad (8)$$

where  $\mathbf{L}^*$  is a weighted Laplacian matrix and defined via

$$\mathbf{L}^* = \mathbf{D}_\mu - \mathbf{A}_\mu$$

with

$$[\mathbf{A}_\mu]_{ij} = \mu_{ij} [\mathbf{A}]_{ij}, j \in N_i$$

$$[\mathbf{D}_\mu]_{ii} = \sum_{j \in N_i} \mu_{ij}, [\mathbf{D}_\mu]_{ij} = 0, \text{ otherwise}$$

In a similar fashion as in [9], the transfer function between  $\dot{\mathbf{q}}$  and  $\mathbf{w}$  is

$$\mathbf{T}(s) = \frac{s\mathbf{I}_{3 \times N}}{s\mathbf{I}_{3 \times N} + \mathbf{L}^* \otimes \mathbf{I}_3} \quad (9)$$

and which has all its poles in the open left half complex plane. This follows from the fact that the weighted Laplacian  $\mathbf{L}^*$  has one zero eigenvalue and all others locate in the open right half complex plane (Ch. 3 in [22]). In particular, one can find that the polynomial  $(s\mathbf{I}_{3 \times N} + \mathbf{L}^* \otimes \mathbf{I}_3)$  has one root at zero and all others are in the open left half complex plane. The remaining arguments are similar to those made in [9] for the node-independent case. By considering the zero-pole cancelation, a stable system for  $\mathbf{w}(t) = \dot{\mathbf{q}} + (\mathbf{L}^* \otimes \mathbf{I}_3)\mathbf{q}$  is achieved. Therefore, with  $\lim_{t \rightarrow \infty} |\mathbf{w}_i| = 0$ , one has  $\lim_{t \rightarrow \infty} |\dot{\mathbf{q}}_i| = 0, i = 1, \dots, N$ .

According to equation (1), one has

$$\lim_{t \rightarrow \infty} |\boldsymbol{\omega}_i| = 0$$

According to Theorem 3 in [27], if the associated communication graph satisfies Assumption 1, the information variables satisfy  $|\mathbf{q}_i(t) - \mathbf{q}_j(t)| \rightarrow 0$  as  $t \rightarrow \infty$  and which concludes the proof.

**Remark 1:** One can easily observe that the node-dependent modification is a special case of edge-dependent modification with  $\mu_{ij} = \mu_i, j \in N_i$  [25].

For the synchronization signal with node-dependent gains given by

$$\mathbf{v}_i(t) \triangleq \dot{\mathbf{q}}_i(t) + \mu_i \sum_{j \in N_i} (\mathbf{q}_i(t) - \mathbf{q}_j(t))$$

and using equation (4), with  $\mu_{ij} = \mu_i$  for all neighbors of node  $i$ , one has

$$\begin{aligned}
\mathbf{w}_i(t) &\triangleq \dot{\mathbf{q}}_i(t) + \sum_{j \in N_i} \mu_{ij} (\mathbf{q}_i(t) - \mathbf{q}_j(t)) = \dot{\mathbf{q}}_i(t) + \sum_{j \in N_i} \mu_i (\mathbf{q}_i(t) - \mathbf{q}_j(t)) \\
&= \dot{\mathbf{q}}_i(t) + \mu_i \sum_{j \in N_i} (\mathbf{q}_i(t) - \mathbf{q}_j(t)) = \mathbf{v}_i(t)
\end{aligned}$$

The above can also be adapted for the special uniform case with  $\mu_{ij} = \mu, j \in N_i$ . For the synchronization signal with constant synchronization gains [9] defined by

$$\mathbf{z}_i(t) \triangleq \dot{\mathbf{q}}_i(t) + \mu \sum_{j \in N_i} (\mathbf{q}_i(t) - \mathbf{q}_j(t))$$

if take  $\mu_{ij} = \mu, \forall i = 1, \dots, N$  and  $j \in N_i$  in equation (4), one has

$$\begin{aligned}
\mathbf{w}_i(t) &\triangleq \dot{\mathbf{q}}_i(t) + \sum_{j \in N_i} \mu_{ij} (\mathbf{q}_i(t) - \mathbf{q}_j(t)) = \dot{\mathbf{q}}_i(t) + \sum_{j \in N_i} \mu (\mathbf{q}_i(t) - \mathbf{q}_j(t)) \\
&= \dot{\mathbf{q}}_i(t) + \mu \sum_{j \in N_i} (\mathbf{q}_i(t) - \mathbf{q}_j(t)) = \mathbf{z}_i(t)
\end{aligned}$$

### 3.2 Adaptation of synchronization penalty terms for Edge-dependent gains

Now consider the adaptive adjustment of the edge-dependent synchronization gains in the synchronization signal defined as equation (3)

$$\mathbf{y}_i(t) = \dot{\mathbf{q}}_i(t) + \sum_{j \in N_i} \lambda_{ij}^* (\mathbf{q}_i(t) - \mathbf{q}_j(t)), \quad i = 1, \dots, N \quad (10)$$

The edge-dependent synchronization gains  $\lambda_{ij}^* > 0$  are fixed for the definition of the synchronization signal  $\mathbf{y}_i$  in (10), but the equivalent synchronization gains in the definition of the control torque (5), will be time-dependent. Choose the following control law for system (2) which includes the time-varying edge-dependent synchronization gains  $\lambda_{ij}(t)$  [25]

$$\begin{aligned}
\boldsymbol{\tau}_i &= -\mathbf{M}_i \sum_{j \in N_i} \lambda_{ij}(t) \dot{\mathbf{q}}_{ij} - \mathbf{C}_i \sum_{j \in N_i} \lambda_{ij}(t) \mathbf{q}_{ij} - \boldsymbol{\tau}_{ext,i} + \bar{\boldsymbol{\tau}}_i \\
&= -\mathbf{M}_i \sum_{j \in N_i} (\lambda_{ij}^* + \tilde{\lambda}_{ij}(t)) \dot{\mathbf{q}}_{ij} - \mathbf{M}_i \sum_{j \in N_i} (\lambda_{ij}^* + \tilde{\lambda}_{ij}(t)) \mathbf{q}_{ij} - \boldsymbol{\tau}_{ext,i} + \bar{\boldsymbol{\tau}}_i \\
&= -\sum_{j \in N_i} \lambda_{ij}^* (\mathbf{M}_i \dot{\mathbf{q}}_{ij} + \mathbf{C}_i \mathbf{q}_{ij}) - \boldsymbol{\tau}_{ext,i} + \bar{\boldsymbol{\tau}}_i - \sum_{j \in N_i} \tilde{\lambda}_{ij}(t) (\mathbf{M}_i \dot{\mathbf{q}}_{ij} + \mathbf{C}_i \mathbf{q}_{ij}) \quad (11)
\end{aligned}$$

where the parameter errors are given by

$$\tilde{\lambda}_{ij}(t) = \lambda_{ij}(t) - \lambda_{ij}^*, \quad j \in N_i, i = 1, \dots, N$$

with  $\lambda_{ij}^*$  denoting the constant edge-dependent synchronization gains used in (10) for the definition of the synchronization signals  $\mathbf{y}_i(t)$ , and  $\tilde{\lambda}_{ij}(t)$  denoting the time-varying parameter errors.

When (10) and (11) are substituted in (2), one obtains the closed-loop systems expressed in terms of the parameter errors

$$\begin{aligned}
\mathbf{M}_i \left( \dot{\mathbf{y}}_i - \sum_{j \in N_i} \lambda_{ij}^* \dot{\mathbf{q}}_{ij} \right) + \mathbf{C}_i \left( \mathbf{y}_i - \sum_{j \in N_i} \lambda_{ij}^* \mathbf{q}_{ij} \right) &= - \sum_{j \in N_i} \lambda_{ij}^* (\mathbf{M}_i \dot{\mathbf{q}}_{ij} + \mathbf{C}_i \mathbf{q}_{ij}) - \boldsymbol{\tau}_{ext,i} \\
&\quad - \sum_{j \in N_i} \tilde{\lambda}_{ij}(t) (\mathbf{M}_i \dot{\mathbf{q}}_{ij} + \mathbf{C}_i \mathbf{q}_{ij}) + \boldsymbol{\tau}_{ext,i} + \bar{\boldsymbol{\tau}}_i
\end{aligned}$$

or

$$\mathbf{M}_i \dot{\mathbf{y}}_i + \mathbf{C}_i \mathbf{y}_i = - \sum_{j \in N_i} \tilde{\lambda}_{ij}(t) (\mathbf{M}_i \dot{\mathbf{q}}_{ij} + \mathbf{C}_i \mathbf{q}_{ij}) + \bar{\boldsymbol{\tau}}_i, \quad i = 1, \dots, N \quad (12)$$

The above follows the approach used in adaptive control systems where the closed-loop system contains the “desired” dynamics and the parameter errors multiplying the regressor signals. When the parameters are known *i.e* when  $\lambda_{ij}(t)$  are replaced by  $\lambda_{ij}^*$ , thereby resulting in  $\tilde{\lambda}_{ij}(t) = 0$ , one can immediately show stability and convergence for

$\mathbf{M}_i \dot{\mathbf{y}}_i + \mathbf{C}_i \mathbf{y}_i = \bar{\boldsymbol{\tau}}_i$  with  $\bar{\boldsymbol{\tau}}_i = -\mathbf{K}_i \mathbf{y}_i$  as in Section 3.1.

The adaptation of the gains  $\dot{\lambda}_{ij}$ , which is based on Lyapunov-redesign methods, is given by

$$\dot{\lambda}_{ij} = \dot{\tilde{\lambda}}_{ij} = \gamma_{ij} \mathbf{y}_i^T (\mathbf{M}_i \dot{\mathbf{q}}_{ij} + \mathbf{C}_i \mathbf{q}_{ij}), \quad j \in N_i, i = 1, \dots, N \quad (13)$$

where  $\gamma_{ij} > 0$  denote the adaptive gains whose role is to speed up adaptation. Following the possible modifications in adaptive parameter estimation [28], one may also consider the following leakage modification to (13)

$$\dot{\lambda}_{ij} = \dot{\tilde{\lambda}}_{ij} = \gamma_{ij} \mathbf{y}_i^T (\mathbf{M}_i \dot{\mathbf{q}}_{ij} + \mathbf{C}_i \mathbf{q}_{ij}) - \sigma_{ij} \tilde{\lambda}_{ij}, \quad j \in N_i, i = 1, \dots, N \quad (14)$$

where  $\sigma_{ij} > 0$  are the values for the fixed  $\sigma$ -modification [28]. It should be noted that the above modification involves the parameter error  $\tilde{\lambda}_{ij}(t)$ . While in standard adaptive systems one does not have access to the unknown parameters, here the values of  $\lambda_{ij}^*$  used for the definition of (10) are known as they are design parameters. Thus the adaptive modification in (14) is feasible since it uses available signals.

The stability properties of the proposed adaptive system described by (10)-(14) are now examined.

**Theorem 2:** With the synchronization signal defined by (10) and the adaptive control law (11), adaptive law (13) and imposing Assumption 1, the attitude synchronization problem in the sense of (3) can be achieved by choosing  $\bar{\boldsymbol{\tau}}_i = -\mathbf{K}_i \mathbf{y}_i$ , where  $\mathbf{K}_i$  is a positive definite matrix.

*Proof:* Construct a Lyapunov-like function

$$V_i(\mathbf{y}_i, \tilde{\lambda}_{ij}) = \frac{1}{2} \mathbf{y}_i^T \mathbf{M}_i \mathbf{y}_i + \frac{1}{2} \sum_{j \in N_i} \left( \frac{\tilde{\lambda}_{ij}^2}{\gamma_{ij}} \right)$$

Take the derivative of  $V_i$  along the trajectories of (12) and (13)

$$\begin{aligned}
\dot{V}_i &= \frac{1}{2} \mathbf{y}_i^T \dot{\mathbf{M}}_i \mathbf{y}_i + \mathbf{y}_i^T \mathbf{M}_i \dot{\mathbf{y}}_i + \sum_{j \in N_i} \frac{\tilde{\lambda}_{ij} \dot{\tilde{\lambda}}_{ij}}{\gamma_{ij}} \\
&= \frac{1}{2} \mathbf{y}_i^T (\dot{\mathbf{M}}_i - 2\mathbf{C}_i + 2\mathbf{C}_i) \mathbf{y}_i + \mathbf{y}_i^T \left( - \sum_{j \in N_i} \tilde{\lambda}_{ij}(t) (\mathbf{M}_i \dot{\mathbf{q}}_{ij} + \mathbf{C}_i \mathbf{q}_{ij}) + \bar{\boldsymbol{\tau}}_i - \mathbf{C}_i \mathbf{y}_i \right) \\
&\quad + \sum_{j \in N_i} \frac{\tilde{\lambda}_{ij} \dot{\tilde{\lambda}}_{ij}}{\gamma_{ij}} \\
&= \mathbf{y}_i^T \left( - \sum_{j \in N_i} \tilde{\lambda}_{ij}(t) (\mathbf{M}_i \dot{\mathbf{q}}_{ij} + \mathbf{C}_i \mathbf{q}_{ij}) + \bar{\boldsymbol{\tau}}_i \right) + \sum_{j \in N_i} \frac{\tilde{\lambda}_{ij}}{\gamma_{ij}} (\gamma_{ij} \mathbf{y}_i^T (\mathbf{M}_i \dot{\mathbf{q}}_{ij} + \mathbf{C}_i \mathbf{q}_{ij})) \\
&= \mathbf{y}_i^T \bar{\boldsymbol{\tau}}_i + \sum_{j \in N_i} \tilde{\lambda}_{ij} \left[ -\mathbf{y}_i^T (\mathbf{M}_i \dot{\mathbf{q}}_{ij} + \mathbf{C}_i \mathbf{q}_{ij}) + \frac{\gamma_{ij} \mathbf{y}_i^T (\mathbf{M}_i \dot{\mathbf{q}}_{ij} + \mathbf{C}_i \mathbf{q}_{ij})}{\gamma_{ij}} \right] \\
&= \mathbf{y}_i^T \bar{\boldsymbol{\tau}}_i = -\mathbf{y}_i^T \mathbf{K}_i \mathbf{y}_i \leq 0
\end{aligned}$$

Following standard adaptive control stability arguments [28], one has that  $\mathbf{y}_i \in \mathcal{L}_\infty \cap \mathcal{L}_2$ , and  $\tilde{\lambda}_{ij}$  and  $\lambda_{ij} \in \mathcal{L}_\infty$ . Replacing the  $\mu_{ij}$  in (10) by  $\lambda_{ij}^*$  and using the same arguments used in Theorem 1, one has  $\dot{\mathbf{q}}_i \in \mathcal{L}_\infty$  and subsequently  $\mathbf{q}_i \in \mathcal{L}_\infty$ .

Then using the fact that  $\sum_{j \in N_i} \tilde{\lambda}_{ij}(t) \dot{\mathbf{q}}_{ij} \in \mathcal{L}_\infty$  and  $\sum_{j \in N_i} \tilde{\lambda}_{ij}(t) \mathbf{q}_{ij} \in \mathcal{L}_\infty$ , along with properties (P1)-(P3) in (12), one has  $\dot{\mathbf{y}}_i \in \mathcal{L}_\infty$  such that  $\dot{V}_i = -2\mathbf{y}_i^T \mathbf{K}_i \dot{\mathbf{y}}_i \in \mathcal{L}_\infty$ .

With an application of Barbălat's Lemma one has

$$\lim_{t \rightarrow \infty} |\mathbf{y}_i| = 0$$

then

$$\begin{aligned}
\lim_{t \rightarrow \infty} |\dot{\mathbf{q}}_i| &= 0 \\
& \qquad \qquad \qquad i = 1, \dots, N \\
\lim_{t \rightarrow \infty} |\boldsymbol{\omega}_i| &= 0
\end{aligned}$$

Finally, with the aid of Theorem 3 in [27], one has  $\lim_{t \rightarrow \infty} |\mathbf{q}_i(t) - \mathbf{q}_j(t)| \rightarrow 0$ .

When the  $\sigma$ -modification (14) is used in the adaptation of  $\lambda_{ij}(t)$ , then the convergence of  $\tilde{\lambda}_{ij}$  and  $\mathbf{y}_i$  to zero become exponential since one obtains  $\dot{V}_i(\mathbf{y}_i, \tilde{\lambda}_{ij}) \leq -cV_i(\mathbf{y}_i, \tilde{\lambda}_{ij})$ .

The remaining arguments are identical to the above case.

## Chapter 4

# Attitude Synchronization of Spacecraft Formation with Unknown Parameters

Generally, one cannot know exactly the inertial parameters and external disturbances. Thus, one can define  $\hat{\boldsymbol{\theta}}_i(t)$  to estimate the true value of  $\boldsymbol{\theta}_i$ . In this section, the case of unknown parameters is considered.

Similar to Chapter 3, first consider synchronization gains based on the proposed edge-dependent modification. Then, expand it to the adaptive adjustment of edge-dependent consensus gain which result in time-varying gains.

### 4.1 Edge-dependent fixed synchronization gains for parameter uncertainty case

According to Property 4, the dynamics of spacecraft are linearly parameterizable as long as  $\mathbf{d}_{ext}$  is constant. Since the actual constant  $p$ -dimensional vector  $\boldsymbol{\theta}_i$  is unknown, one can generate the estimate of  $\boldsymbol{\theta}_i$  as  $\hat{\boldsymbol{\theta}}_i(t)$  at time  $t$ . Then the following equation holds

$$\mathbf{Y}_i \widehat{\boldsymbol{\theta}}_i = \widehat{\mathbf{M}}_i \sum_{j \in N_i} \mu_{ij} \dot{\mathbf{q}}_{ij} + \widehat{\mathbf{C}}_i \sum_{j \in N_i} \mu_{ij} \mathbf{q}_{ij} + \widehat{\boldsymbol{\tau}}_{ext,i} \quad (15)$$

where  $\widehat{\mathbf{M}}_i, \widehat{\mathbf{C}}_i$  are the adaptive estimates matrices of  $\mathbf{M}_i$  and  $\mathbf{C}_i$  due to the unknown moment of inertia, and  $\widehat{\boldsymbol{\tau}}_{ext,i}$  is the estimate for the external disturbance  $\boldsymbol{\tau}_{ext,i}$ .

For the Euler-Lagrange equation (2), propose the control input for the  $i$ -th spacecraft as

$$\boldsymbol{\tau}_i = -\widehat{\mathbf{M}}_i \sum_{j \in N_i} \mu_{ij} \dot{\mathbf{q}}_{ij} - \widehat{\mathbf{C}}_i \sum_{j \in N_i} \mu_{ij} \mathbf{q}_{ij} - \widehat{\boldsymbol{\tau}}_{ext,i} + \bar{\boldsymbol{\tau}}_i = -\mathbf{Y}_i \widehat{\boldsymbol{\theta}}_i + \bar{\boldsymbol{\tau}}_i, \quad i = 1, \dots, N \quad (16)$$

Introduce the synchronization signal using the edge-dependent modification

$$\mathbf{w}_i(t) \triangleq \dot{\mathbf{q}}_i(t) + \sum_{j \in N_i} \mu_{ij} \mathbf{q}_{ij}(t), \quad i = 1, \dots, N \quad (17)$$

where  $\mathbf{q}_{ij}(t) = \mathbf{q}_i(t) - \mathbf{q}_j(t)$  is the attitude error between the  $i$ -th spacecraft and its neighbors.

Substitute (16) and (17) into (2)

$$\begin{aligned} \mathbf{M}_i \left( \dot{\mathbf{w}}_i - \sum_{j \in N_i} \mu_{ij} \dot{\mathbf{q}}_{ij} \right) + \mathbf{C}_i \left( \mathbf{w}_i - \sum_{j \in N_i} \mu_{ij} \mathbf{q}_{ij} \right) = & -\widehat{\mathbf{M}}_i \sum_{j \in N_i} \mu_{ij} \dot{\mathbf{q}}_{ij} - \widehat{\mathbf{C}}_i \sum_{j \in N_i} \mu_{ij} \mathbf{q}_{ij} \\ & - \widehat{\boldsymbol{\tau}}_{ext,i} + \bar{\boldsymbol{\tau}}_i + \boldsymbol{\tau}_{ext,i} \end{aligned}$$

or

$$\mathbf{M}_i \dot{\mathbf{w}}_i + \mathbf{C}_i \mathbf{w}_i = \mathbf{Y}_i \boldsymbol{\theta}_i - \mathbf{Y}_i \widehat{\boldsymbol{\theta}}_i + \bar{\boldsymbol{\tau}}_i$$

The closed-loop system is given by

$$\mathbf{M}_i \dot{\mathbf{w}}_i + \mathbf{C}_i \mathbf{w}_i = \mathbf{Y}_i \tilde{\boldsymbol{\theta}}_i + \bar{\boldsymbol{\tau}}_i \quad (18)$$

where  $\tilde{\boldsymbol{\theta}}_i = \boldsymbol{\theta}_i - \widehat{\boldsymbol{\theta}}_i$  is the parameter estimation error, and it evolves as

$$\dot{\tilde{\boldsymbol{\theta}}}_i = -\dot{\widehat{\boldsymbol{\theta}}}_i = -\boldsymbol{\Gamma}_i^{-1} \mathbf{Y}_i^T \mathbf{w}_i, \quad i = 1, \dots, N \quad (19)$$

**Theorem 3:** Assuming fixed communication topology via Assumption 1, and the proposed control architecture described by (16) and (17), the resulting closed loop system

(18) along with the adaptive laws (19) and the control law  $\bar{\tau}_i = -\mathbf{K}_i \mathbf{w}_i$ , where  $\mathbf{K}_i$  is a positive definite diagonal matrix solve the attitude synchronization in the sense of (3).

*Proof:* Consider the following Lyapunov-like function

$$V_i(\mathbf{w}_i, \tilde{\boldsymbol{\theta}}_i) = \frac{1}{2} \mathbf{w}_i^T \mathbf{M}_i \mathbf{w}_i + \frac{1}{2} \tilde{\boldsymbol{\theta}}_i^T \boldsymbol{\Gamma}_i \tilde{\boldsymbol{\theta}}_i, \quad i = 1, \dots, N$$

Using Property (P2) and (P4), take the derivative of  $V_i$  along the trajectory of (18) and (19)

$$\begin{aligned} \dot{V}_i &= \frac{1}{2} \mathbf{w}_i^T \dot{\mathbf{M}}_i \mathbf{w}_i + \mathbf{w}_i^T \mathbf{M}_i \dot{\mathbf{w}}_i + \tilde{\boldsymbol{\theta}}_i^T \boldsymbol{\Gamma}_i \dot{\tilde{\boldsymbol{\theta}}}_i \\ &= \frac{1}{2} \mathbf{w}_i^T (\dot{\mathbf{M}}_i - 2\mathbf{C}_i + 2\mathbf{C}_i) \mathbf{w}_i + \mathbf{w}_i^T (\mathbf{Y}_i \tilde{\boldsymbol{\theta}}_i + \bar{\tau}_i - \mathbf{C}_i \mathbf{w}_i) - \tilde{\boldsymbol{\theta}}_i^T \boldsymbol{\Gamma}_i \dot{\tilde{\boldsymbol{\theta}}}_i \\ &= \mathbf{w}_i^T \bar{\tau}_i + \tilde{\boldsymbol{\theta}}_i^T (\mathbf{Y}_i^T \mathbf{w}_i - \boldsymbol{\Gamma}_i \dot{\tilde{\boldsymbol{\theta}}}_i) = -\mathbf{w}_i^T \mathbf{K}_i \mathbf{w}_i + \tilde{\boldsymbol{\theta}}_i^T (\mathbf{Y}_i^T \mathbf{w}_i - \boldsymbol{\Gamma}_i \boldsymbol{\Gamma}_i^{-1} \mathbf{Y}_i^T \mathbf{w}_i) \\ &= -\mathbf{w}_i^T \mathbf{K}_i \mathbf{w}_i \leq 0 \end{aligned}$$

Following standard control stability arguments [26] [28], one has that since  $V_i \geq 0$ ,  $\dot{V}_i \leq 0$ , then  $V_i$  is bounded indicating  $\mathbf{w}_i \in \mathcal{L}_\infty \cap \mathcal{L}_2$ ,  $\tilde{\boldsymbol{\theta}}$  and  $\hat{\boldsymbol{\theta}}_i \in \mathcal{L}_\infty$ .

Using the same arguments as in Chapter 3, one has  $\dot{\mathbf{q}}_i \in \mathcal{L}_\infty$  and  $\sum_{j \in N_i} \dot{\mathbf{q}}_{ij} \in \mathcal{L}_\infty$ . According to (17),  $\sum_{j \in N_i} \mathbf{q}_{ij} \in \mathcal{L}_\infty$  and  $\mathbf{q}_i \in \mathcal{L}_\infty$ . With respect to equation (15) and property (P1) and (P3),  $\mathbf{Y}_i \in \mathcal{L}_\infty$ . According to equation (18), one has  $\dot{\mathbf{w}}_i \in \mathcal{L}_\infty$ .

Then

$$\ddot{V}_i = -2\mathbf{w}_i^T \mathbf{K}_i \dot{\mathbf{w}}_i \in \mathcal{L}_\infty$$

and along with Barbălat's lemma, one arrives at

$$\lim_{t \rightarrow \infty} \dot{V}_i = 0, \quad \lim_{t \rightarrow \infty} \mathbf{w}_i = 0$$

such that

$$\lim_{t \rightarrow \infty} \dot{\mathbf{q}}_i = 0, \quad \lim_{t \rightarrow \infty} \boldsymbol{\omega}_i = 0$$

From Theorem 3 in [27], one has  $|\mathbf{q}_j(t) - \mathbf{q}_i(t)| \rightarrow 0$ , as  $t \rightarrow \infty$ .

#### 4.2 Edge-dependent time-varying gains for the parameter uncertainty case

Now consider the adaptive adjustment of edge-dependent consensus gains  $\lambda_{ij}(t)$ . Define the synchronization signal

$$\mathbf{y}_i(t) \triangleq \dot{\mathbf{q}}_i(t) + \sum_{j \in N_i} \lambda_{ij}^* (\mathbf{q}_i(t) - \mathbf{q}_j(t)) \quad (20)$$

Here, the edge-dependent synchronization gains  $\lambda_{ij}^* > 0$  are fixed.

Choose the control input as

$$\begin{aligned} \boldsymbol{\tau}_i &= -\widehat{\mathbf{M}}_i \sum_{j \in N_i} \lambda_{ij}(t) \dot{\mathbf{q}}_{ij} - \widehat{\mathbf{C}}_i \sum_{j \in N_i} \lambda_{ij}(t) \mathbf{q}_{ij} - \widehat{\boldsymbol{\tau}}_{ext,i} + \bar{\boldsymbol{\tau}}_i \\ &= -\widehat{\mathbf{M}}_i \sum_{j \in N_i} (\lambda_{ij}^* + \tilde{\lambda}_{ij}(t)) \dot{\mathbf{q}}_{ij} - \widehat{\mathbf{C}}_i \sum_{j \in N_i} (\lambda_{ij}^* + \tilde{\lambda}_{ij}(t)) \mathbf{q}_{ij} - \widehat{\boldsymbol{\tau}}_{ext,i} + \bar{\boldsymbol{\tau}}_i \\ &= -\mathbf{Y}_i \widehat{\boldsymbol{\theta}}_i - \sum_{j \in N_i} \tilde{\lambda}_{ij}(t) (\widehat{\mathbf{M}}_i \dot{\mathbf{q}}_{ij} + \widehat{\mathbf{C}}_i \mathbf{q}_{ij}) + \bar{\boldsymbol{\tau}}_i \end{aligned} \quad (21)$$

where the time-varying parameter error are given by

$$\tilde{\lambda}_{ij}(t) = \lambda_{ij}(t) - \lambda_{ij}^*, \quad j \in N_i, i = 1, \dots, N$$

Substitute (20) and (21) into (2)

$$\begin{aligned} \mathbf{M}_i \left( \dot{\mathbf{y}}_i - \sum_{j \in N_i} \lambda_{ij}^* \dot{\mathbf{q}}_{ij} \right) + \mathbf{C}_i \left( \mathbf{y}_i - \sum_{j \in N_i} \lambda_{ij}^* \mathbf{q}_{ij} \right) &= -\widehat{\mathbf{M}}_i \sum_{j \in N_i} (\lambda_{ij}^* + \tilde{\lambda}_{ij}(t)) \dot{\mathbf{q}}_{ij} \\ &\quad - \widehat{\mathbf{C}}_i \sum_{j \in N_i} (\lambda_{ij}^* + \tilde{\lambda}_{ij}(t)) \mathbf{q}_{ij} - \widehat{\boldsymbol{\tau}}_{ext,i} + \bar{\boldsymbol{\tau}}_i + \boldsymbol{\tau}_{ext,i} \end{aligned}$$

the closed-loop system is obtained

$$\mathbf{M}_i \dot{\mathbf{y}}_i + \mathbf{C}_i \mathbf{y}_i = \mathbf{Y}_i \tilde{\boldsymbol{\theta}}_i - \widehat{\mathbf{M}}_i \sum_{j \in N_i} \tilde{\lambda}_{ij} \dot{\mathbf{q}}_{ij} - \widehat{\mathbf{C}}_i \sum_{j \in N_i} \tilde{\lambda}_{ij} \mathbf{q}_{ij} + \bar{\boldsymbol{\tau}}_i \quad (22)$$

where  $\tilde{\boldsymbol{\theta}}_i = \boldsymbol{\theta}_i - \hat{\boldsymbol{\theta}}_i$  is the parameter estimation error and is updated via

$$\dot{\tilde{\boldsymbol{\theta}}}_i = -\dot{\hat{\boldsymbol{\theta}}}_i = -\boldsymbol{\Gamma}_i^{-1} \mathbf{Y}_i^T \mathbf{y}_i, \quad i = 1, \dots, N \quad (23)$$

and the gain error  $\tilde{\lambda}_{ij}$  is updated via

$$\dot{\tilde{\lambda}}_{ij} = \gamma_{ij} \mathbf{y}_i^T (\hat{\mathbf{M}}_i \dot{\mathbf{q}}_{ij} + \hat{\mathbf{C}}_i \mathbf{q}_{ij}), \quad j \in N_i, i = 1, \dots, N \quad (24)$$

Alternatively, it can be modified to include a diffusion term

$$\dot{\tilde{\lambda}}_{ij} = \gamma_{ij} \mathbf{y}_i^T (\hat{\mathbf{M}}_i \dot{\mathbf{q}}_{ij} + \hat{\mathbf{C}}_i \mathbf{q}_{ij}) - \sigma_{ij} \tilde{\lambda}_{ij}$$

where  $\gamma_{ij}$  and  $\sigma_{ij}$  are positive adaptive gains [28].

**Theorem 4:** With control architecture (22), adaptive laws (23) and (24) and imposing Assumption 1, the attitude synchronization in the sense of (3) is achieved by choosing  $\bar{\boldsymbol{\tau}}_i = -\mathbf{K}_i \mathbf{y}_i$ , where  $\mathbf{K}_i$  is a positive definite diagonal matrix.

*Proof:* Construct a Lyapunov-like function

$$V_i(\mathbf{y}_i, \tilde{\boldsymbol{\theta}}_i, \tilde{\lambda}_{ij}) = \frac{1}{2} \mathbf{y}_i^T \mathbf{M}_i \mathbf{y}_i + \frac{1}{2} \tilde{\boldsymbol{\theta}}_i^T \boldsymbol{\Gamma}_i \tilde{\boldsymbol{\theta}}_i + \frac{1}{2} \sum_{j \in N_i} \left( \frac{\tilde{\lambda}_{ij}^2}{\gamma_{ij}} \right)$$

Take the derivative of  $V_i$  along the trajectory of (22) (23) and (24), using property (P2) and (P4) to get

$$\begin{aligned} \dot{V}_i &= \frac{1}{2} \mathbf{y}_i^T \dot{\mathbf{M}}_i \mathbf{y}_i + \mathbf{y}_i^T \mathbf{M}_i \dot{\mathbf{y}}_i + \tilde{\boldsymbol{\theta}}_i^T \boldsymbol{\Gamma}_i \dot{\tilde{\boldsymbol{\theta}}}_i + \sum_{j \in N_i} \frac{\tilde{\lambda}_{ij} \dot{\tilde{\lambda}}_{ij}}{\gamma_{ij}} \\ &= \frac{1}{2} \mathbf{y}_i^T (\dot{\mathbf{M}}_i - 2\mathbf{C}_i + 2\mathbf{C}_i) \mathbf{y}_i \\ &\quad + \mathbf{y}_i^T \left( \mathbf{Y}_i \tilde{\boldsymbol{\theta}}_i - \hat{\mathbf{M}}_i \sum_{j \in N_i} \tilde{\lambda}_{ij} \dot{\mathbf{q}}_{ij} - \hat{\mathbf{C}}_i \sum_{j \in N_i} \tilde{\lambda}_{ij} \mathbf{q}_{ij} + \bar{\boldsymbol{\tau}}_i - \mathbf{C}_i \mathbf{y}_i \right) - \tilde{\boldsymbol{\theta}}_i^T \boldsymbol{\Gamma}_i \dot{\hat{\boldsymbol{\theta}}}_i + \sum_{j \in N_i} \frac{\tilde{\lambda}_{ij} \dot{\tilde{\lambda}}_{ij}}{\gamma_{ij}} \\ &= \mathbf{y}_i^T \left( \mathbf{Y}_i \tilde{\boldsymbol{\theta}}_i - \hat{\mathbf{M}}_i \sum_{j \in N_i} \tilde{\lambda}_{ij} \dot{\mathbf{q}}_{ij} - \hat{\mathbf{C}}_i \sum_{j \in N_i} \tilde{\lambda}_{ij} \mathbf{q}_{ij} + \bar{\boldsymbol{\tau}}_i \right) - \tilde{\boldsymbol{\theta}}_i^T \boldsymbol{\Gamma}_i \dot{\hat{\boldsymbol{\theta}}}_i + \sum_{j \in N_i} \frac{\tilde{\lambda}_{ij} \dot{\tilde{\lambda}}_{ij}}{\gamma_{ij}} \\ &= -\mathbf{y}_i^T \mathbf{K}_i \mathbf{y}_i + \tilde{\boldsymbol{\theta}}_i^T (\mathbf{Y}_i^T \mathbf{y}_i - \boldsymbol{\Gamma}_i \boldsymbol{\Gamma}_i^{-1} \mathbf{Y}_i^T \mathbf{y}_i) \end{aligned}$$

$$\begin{aligned}
& + \sum \tilde{\lambda}_{ij} \left[ -\mathbf{y}_i^T (\hat{\mathbf{M}}_i \dot{\mathbf{q}}_{ij} + \hat{\mathbf{C}}_i \mathbf{q}_{ij}) + \frac{\gamma_{ij} \mathbf{y}_i^T (\hat{\mathbf{M}}_i \dot{\mathbf{q}}_{ij} + \hat{\mathbf{C}}_i \mathbf{q}_{ij})}{\gamma_{ij}} \right] \\
& = -\mathbf{y}_i^T \mathbf{K}_i \mathbf{y}_i \leq 0
\end{aligned}$$

Since  $V_i \geq 0$  and  $\dot{V}_i \leq 0$ , then  $\mathbf{y}_i \in \mathcal{L}_\infty \cap \mathcal{L}_2$ ,  $\tilde{\boldsymbol{\theta}}$  and  $\hat{\boldsymbol{\theta}}_i \in \mathcal{L}_\infty$ ,  $\tilde{\lambda}_{ij}$  and  $\lambda_{ij} \in \mathcal{L}_\infty$ .

Using the same arguments as in Theorem 3, then  $\dot{\mathbf{q}} \in \mathcal{L}_\infty$ ,  $\sum_{j \in N_i} \dot{\mathbf{q}}_{ij} \in \mathcal{L}_\infty$ ;  $\sum_{j \in N_i} \mathbf{q}_{ij} \in \mathcal{L}_\infty$  and  $\mathbf{Y}_i \in \mathcal{L}_\infty$ .

According to (22), one has  $\dot{\mathbf{y}}_i \in \mathcal{L}_\infty$ . Finally, for  $j \in N_i, i = 1, \dots, N$ , it can be concluded

$$\ddot{V}_i = -2\mathbf{y}_i^T \mathbf{K}_i \dot{\mathbf{y}}_i \in \mathcal{L}_\infty$$

According to Barbălat's lemma

$$\lim_{t \rightarrow \infty} \dot{V}_i = 0, \quad \lim_{t \rightarrow \infty} \mathbf{y}_i = 0$$

then

$$\lim_{t \rightarrow \infty} |\dot{\mathbf{q}}_i| = 0, \quad \lim_{t \rightarrow \infty} |\boldsymbol{\omega}_i| = 0$$

According to Theorem 3 in [27],  $\lim_{t \rightarrow \infty} |\mathbf{q}_j(t) - \mathbf{q}_i(t)| = 0, j \in N_i, i = 1, \dots, N$ .

# Chapter 5

## Numerical Simulation

In this chapter, numerical simulations are presented to further support the theoretical predictions presented in Chapter 3 and 4. Additionally, the numerical studies help provide insights on the choice of optimal gains by penalizing a combination of the deviation-from-the-mean and the rotational kinetic energy.

Appropriate measures for the synchronization are (i) the deviation-from-the-mean  $\Delta(t)$  and (ii) the rotational kinetic energy  $E_r(t)$ . The optimization of the consensus gains should provide a balance between success of synchronization (low value of  $\|\Delta(t)\|$ ) and controller performance (low value of  $E_r(t)$ ), *i.e.* the synchronization gains should be chosen to minimize the  $L_2(0, t)$  norm of the sum of the rotational kinetic energy and the deviation-from-the-mean

$$\text{optimal gain} = \arg \min \int_0^t (\|\Delta(\tau)\|^2 + E_r^2(\tau)) d\tau \quad (25)$$

where

$$\Delta(t)_{3N \times 1} = \begin{pmatrix} \mathbf{q}_1(t) - \frac{1}{N} \sum_{j=1}^N \mathbf{q}_j(t) \\ \mathbf{q}_2(t) - \frac{1}{N} \sum_{j=1}^N \mathbf{q}_j(t) \\ \vdots \\ \mathbf{q}_N(t) - \frac{1}{N} \sum_{j=1}^N \mathbf{q}_j(t) \end{pmatrix},$$

$$\|\Delta(t)\|^2 \triangleq \sum_{i=1}^N |\delta_i(t)|^2 = \sum_{i=1}^N \left| \mathbf{q}_i(t) - \frac{1}{N} \sum_{j=1}^N \mathbf{q}_j(t) \right|^2$$

$$E_r^2(t) \triangleq \sum_{i=1}^N \boldsymbol{\omega}_i^T(t) \mathbf{J}_i \boldsymbol{\omega}_i(t)$$

It should also be noted that the optimization (25) can be used for selecting the constant gains  $\lambda_{ij}^*$  in the adaptive control law (10) and (11).

### 5.1 Numerical study for the case of known parameters

To demonstrate the effectiveness of the proposed scheme, consider a group of 4 spacecraft with a communication topology depicted in Figure 4.

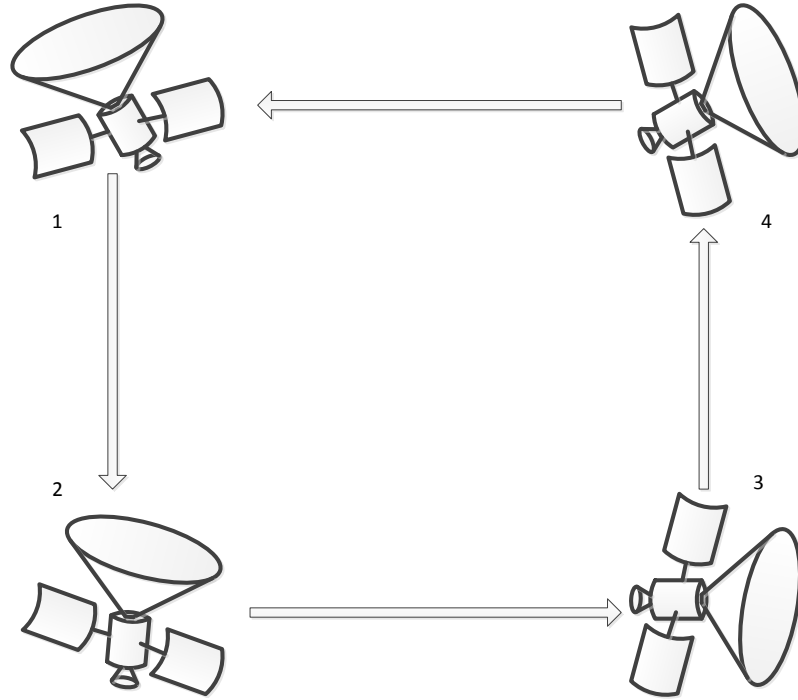


**Figure 3: Section 5.1 Directed graph on 4 spacecraft.**

The corresponding graph Laplacian matrix is given by

$$L(G) = \begin{bmatrix} 1 & 0 & 0 & -1 \\ -1 & 1 & 0 & 0 \\ 0 & -1 & 1 & 0 \\ 0 & 0 & -1 & 1 \end{bmatrix}$$

The initial conditions of these 4 spacecraft are

$$\mathbf{q}_1(0) = [3.0 \quad 2.0 \quad 1.0]^T, \quad \mathbf{q}_2(0) = [3.2 \quad 2.4 \quad 1.9]^T,$$

$$\mathbf{q}_3(0) = [2.7 \quad 1.2 \quad 2.9]^T, \quad \mathbf{q}_4(0) = [5.1 \quad 4.2 \quad 4.0]^T.$$

and the inertia matrices of each spacecraft were chosen as

$$J_1 = \text{diag}(17,12,9), \quad J_2 = \text{diag}(14,13,10),$$

$$J_3 = \text{diag}(20,10,9), \quad J_4 = \text{diag}(15,9,16).$$

Simulation regarding the regulation case is implemented.

### 5.1.1 Effect of constant synchronization gains on system performance

As a prelude to the optimization (25) above, one way to examine the effects of different gains  $\mu_{ij}$  in (5) (6), is to choose the synchronization gains in terms of the initial mismatch of the spacecraft states as follows

$$\mu_{ij} = \alpha_{ij} \cdot |\mathbf{q}_i(0) - \mathbf{q}_j(0)|, \quad i = 1, \dots, N, j \in N_i$$

where  $\alpha_{ij} > 0$  is a positive coefficient presenting the proportion of  $\mu_{ij}$  to the norm  $|\mathbf{q}_{ij}(0)|$ . For the numerical results section, consider these coefficients to be independent of the nodes, that is  $\alpha_{ij} = \alpha$ . In this case, the optimization simplifies to

$$\alpha = \arg \min \int_0^t (\|\Delta(\tau)\|^2 + E_r^2(\tau)) d\tau$$

$$\mu_{ij} = \alpha \cdot |\mathbf{q}_i(0) - \mathbf{q}_j(0)|, \quad i = 1, \dots, N, j \in N_i \quad (26)$$

Use the control structure constructed in Section 3.1. Choose  $\mu_{ij} = 0.2|\mathbf{q}_{ij}(0)|$  (*i.e.*

$$\mu_{12} = 0.8544, \mu_{23} = 0.2010, \mu_{34} = 0.3280, \mu_{41} = 0.7992), K_i = \text{diag}(2,2,2),$$

$i = 1, \dots, N, j \in N_i$ . The synchronization result is depicted in Figure 4 and Figure 5.

Figure 4 shows the convergences of attitude error of spacecraft 2, 3 and 4 with respect to spacecraft 1. Figure 5 indicates the synchronization of angular velocity.

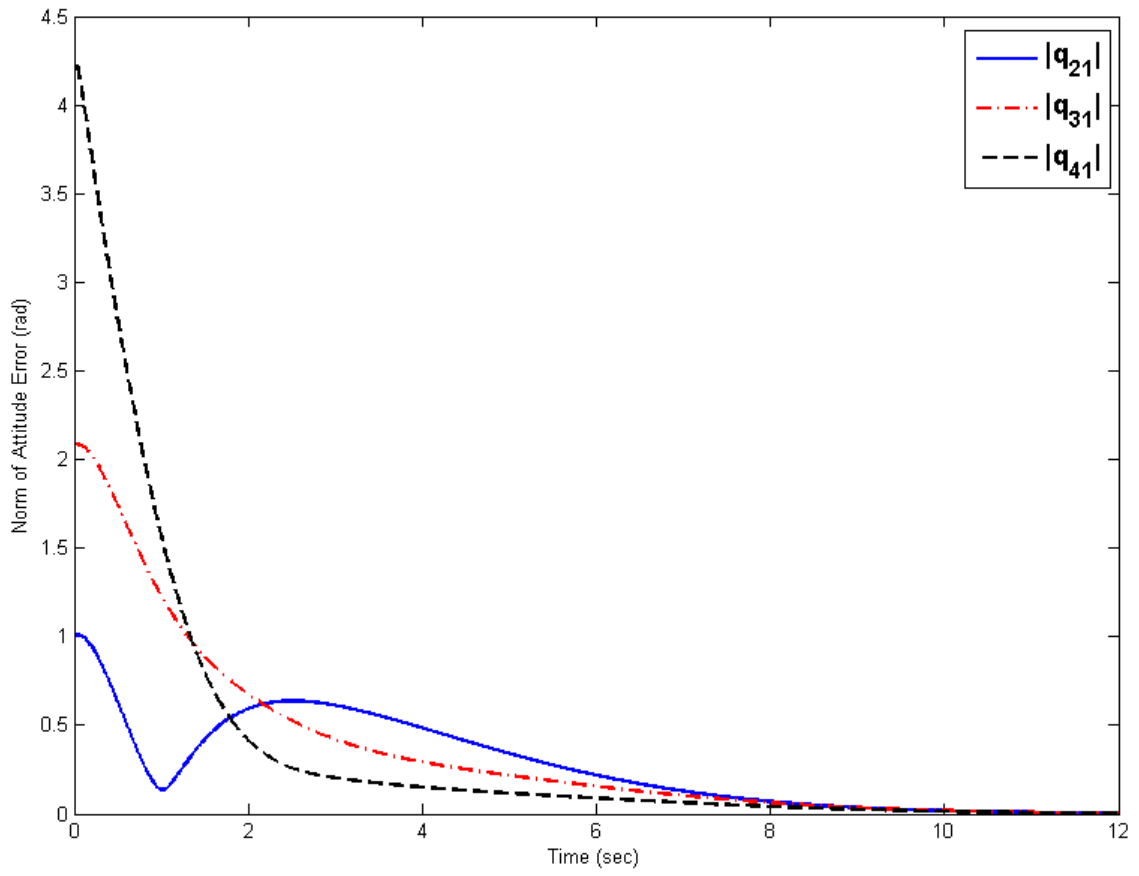


**Figure 4: Section 5.1.1 Evolution of attitude error with constant edge-dependent gain.**

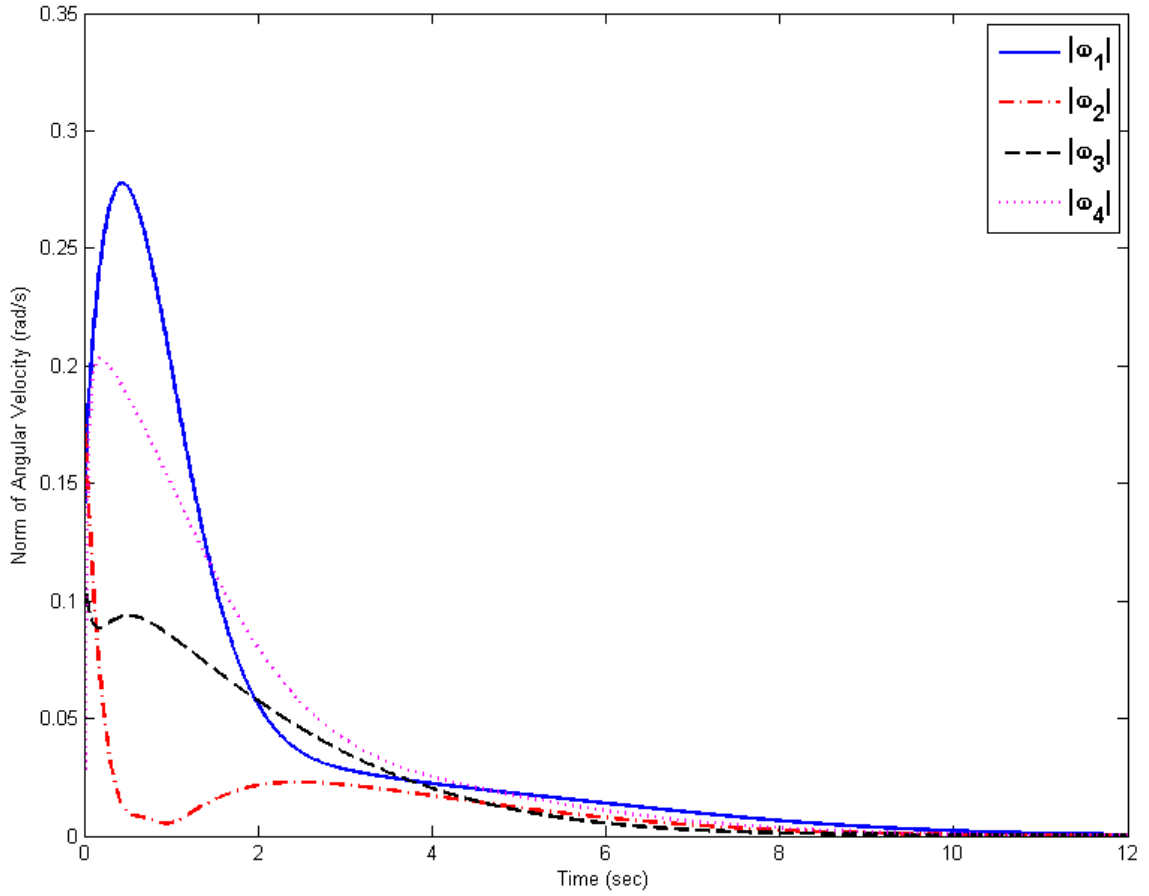


**Figure 5: Section 5.1.1 Evolution of angular velocity with constant edge-dependent gain.**

Figure 6 shows the improvement of edge-dependent gains  $\mu_{ij}$  based on (26) over a uniform gain with a value of  $\mu = 2$ . It examines the effects of both synchronization gains on the sum of  $\|\Delta(t)\|$  and  $E_r(t)$ . These numerical studies reveal that consensus gains chosen in proportion to the initial mismatch between the spacecraft states give out much more satisfactory results than arbitrary weights.

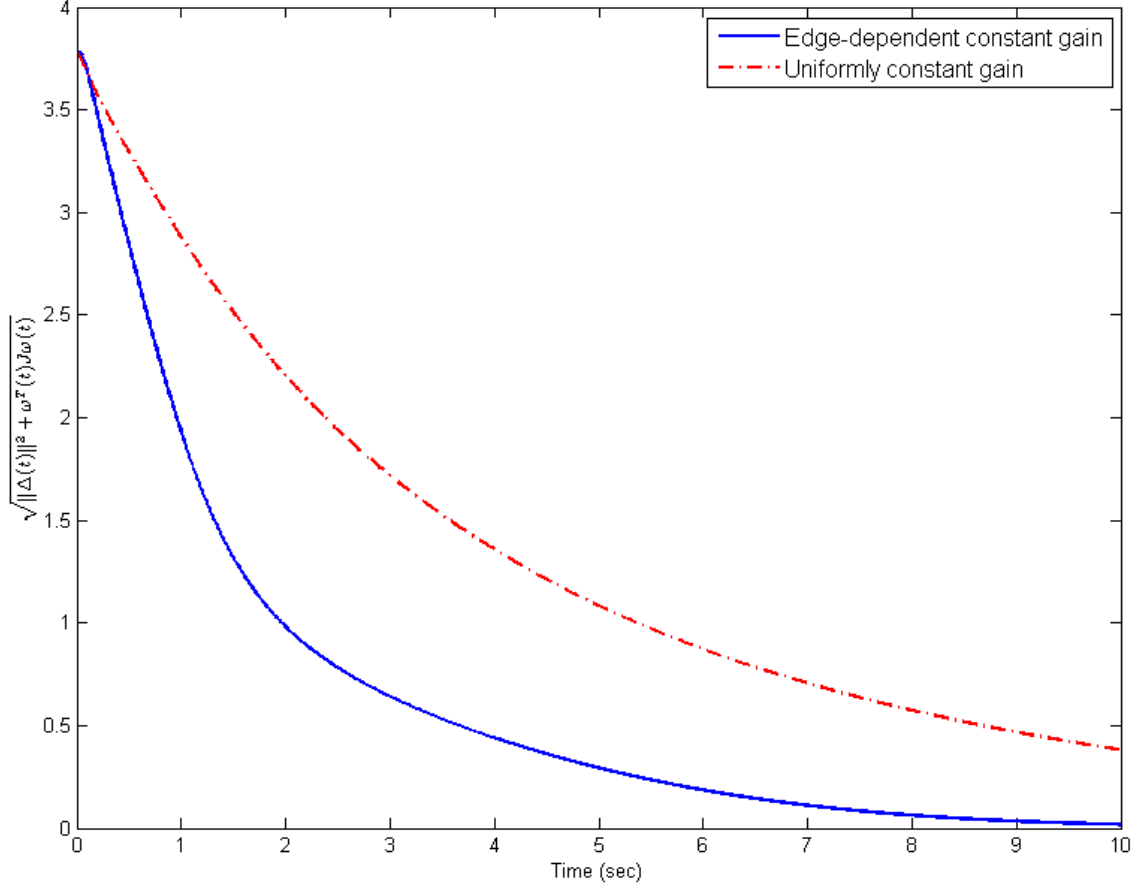


**Figure 6: Section 5.1.1 Evolution of  $\sqrt{\|\Delta(t)\|^2 + E_r^2(t)}$ .**

The sensitivity of the synchronization gains and their effects on the control performance is the focus of the next numerical study.

First, different values of the uniform gain  $\mu$  in the range  $0 < \mu \leq 6$  were considered, see Figure 7. For each value  $\mu \in (0,6]$ , the controller in (4) was implemented and the closed-loop systems (6) were simulated over the time interval  $[0,10]$ s. Both  $L_2(0,10; \mathbb{R}^{3N})$  norm of  $\Delta(t)$  and  $L_2(0,10; \mathbb{R}^1)$  norm of  $E_r(t)$  were calculated for each  $\mu \in (0,6]$ . Figure 7 clearly shows that as the gain  $\mu$  increases, the deviation  $\Delta(t)$  decreases while the rotational kinetic energy  $E_r(t)$  increases. Therefore, an optimal value of the synchronization gain  $\mu$  should compensate for small  $\Delta(t)$  and small kinetic energy. As

one can see from the figure, the intersection point  $\mu = 2.08$  provides good balance between these two performance metrics.

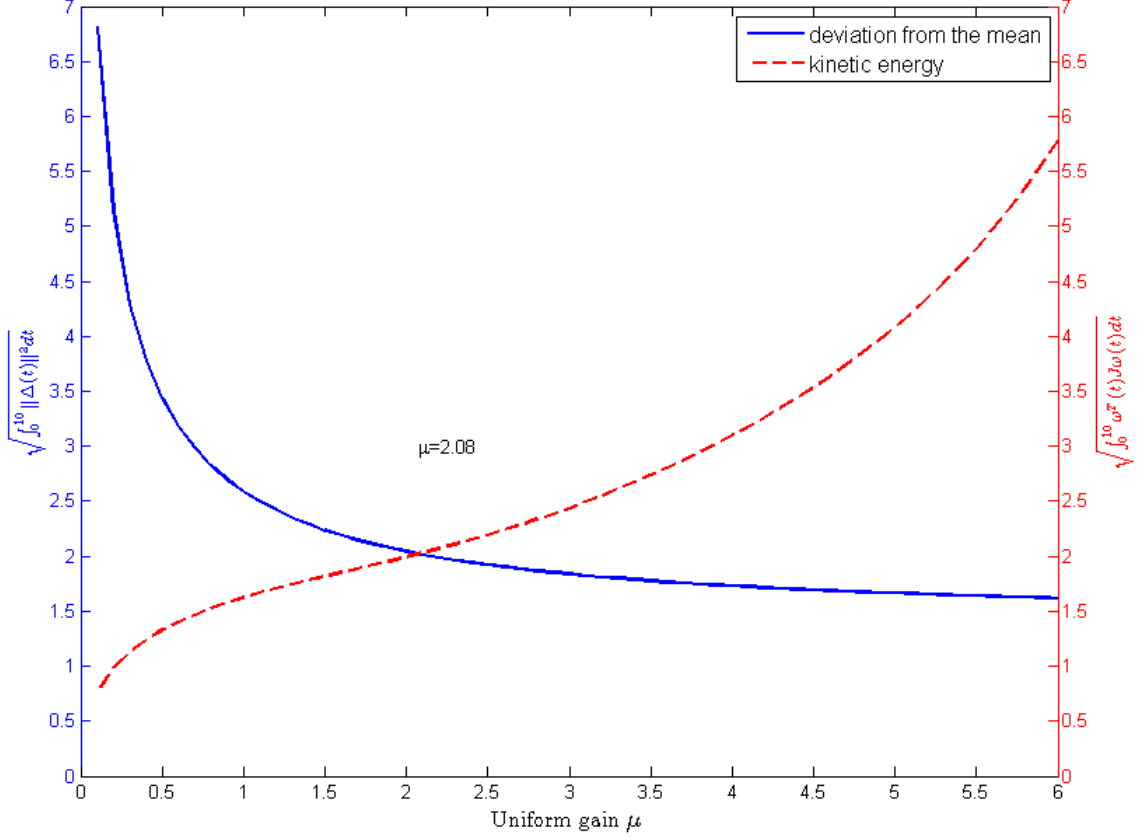


**Figure 7: Section 5.1.1 The effects of varying the uniform fixed gain in the range  $0 < \mu \leq 6$  on  $\|\Delta(t)\|$  and  $E_r(t)$ .**

### 5.1.2 Effect of adaptation of synchronization gains

A study of the adaptation of the synchronizing gain  $\lambda_{ij}(t)$  as given by (10) (11) and (14) is considered. In this case, choose  $\lambda_{ij}^* = 0.5|\mathbf{q}_i(0) - \mathbf{q}_j(0)|, i = 1, \dots, 4, j \in N_i$  in (10), and  $\lambda_{ij}(0) = \lambda_{ij}^*, \gamma_{ij} = 0.005, \sigma_{ij} = 1$  in (15). The following figure shows the synchronization results of the case of adaptive synchronization gains.

Figure 8 and Figure 9 show the convergence of attitude error of spacecraft 2, 3 and 4 with respect to spacecraft 1, and the convergence of angular velocity respectively.

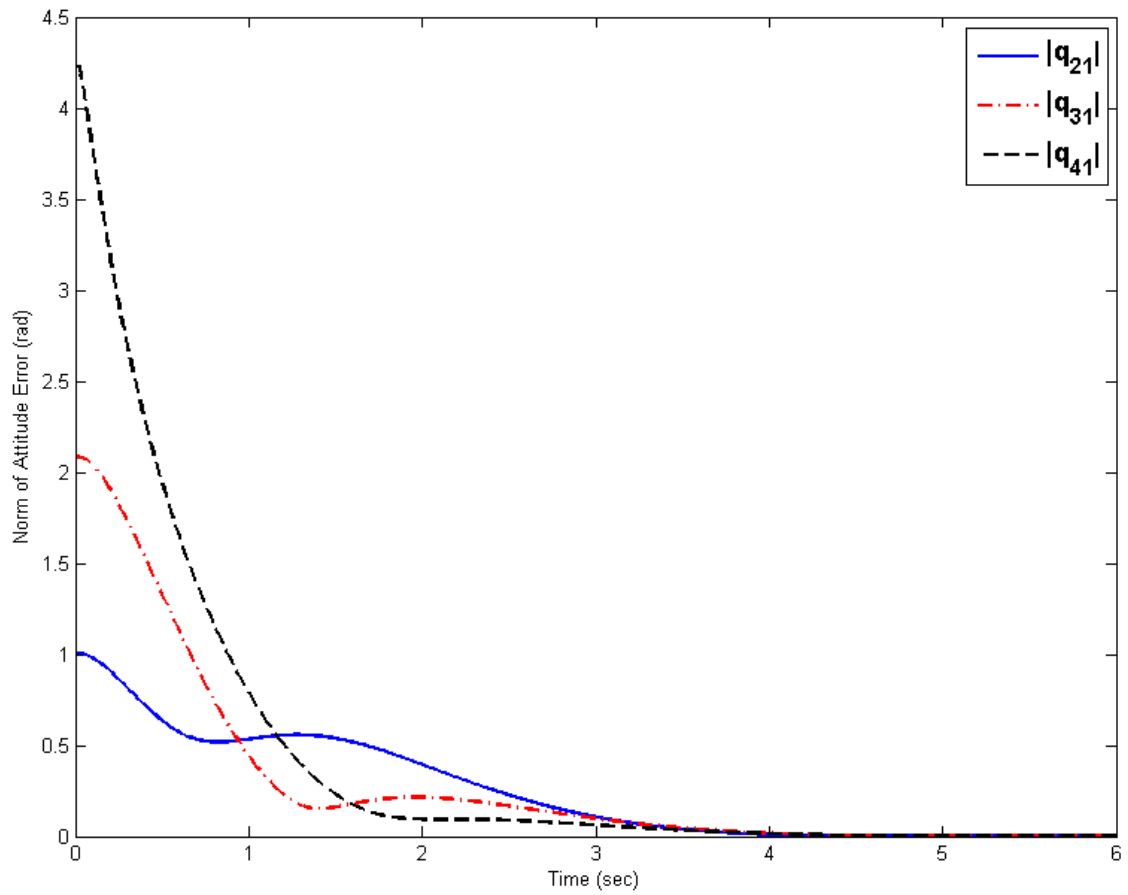


**Figure 8: Section 5.1.2 Evolution of attitude error with adaptive edge-dependent gain.**

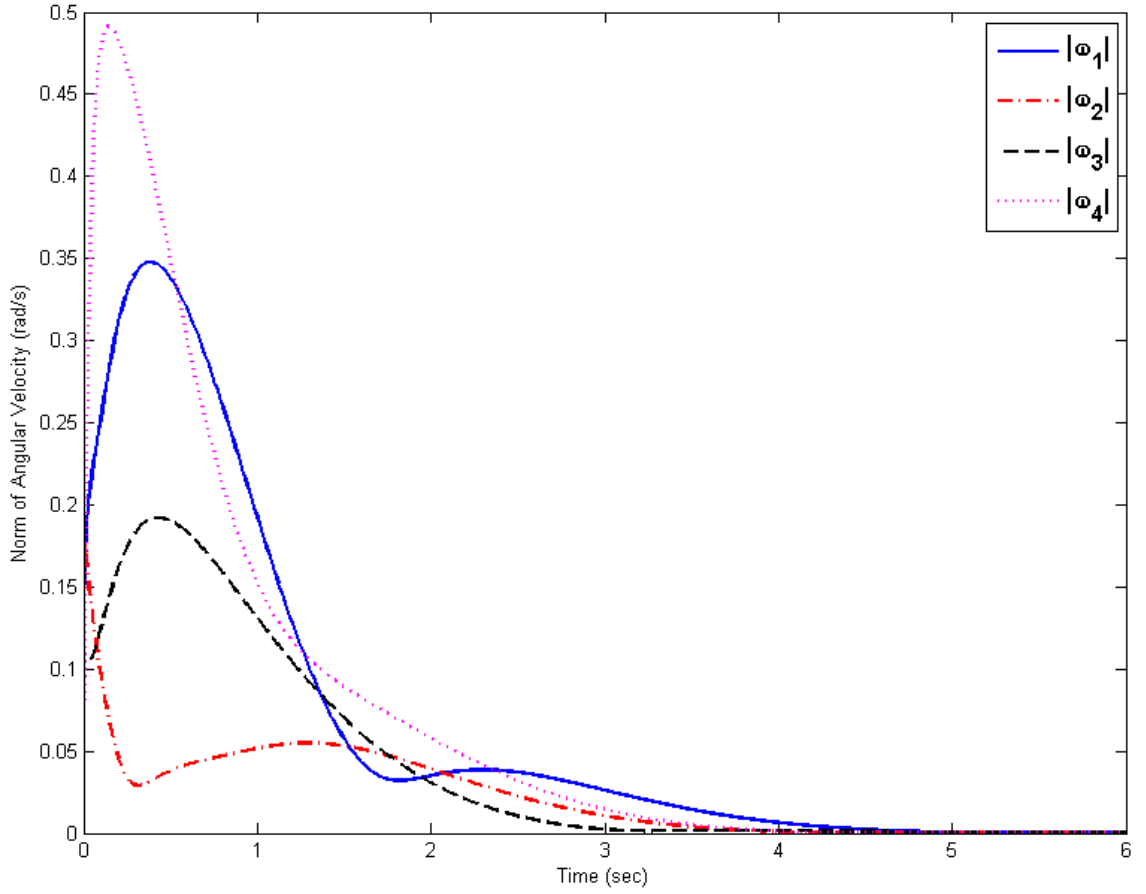


**Figure 9: Section 5.1.2 Evolution of angular velocity with adaptive edge-dependent gain.**

The result depicted in Figure 10, which compares the cumulative effect of  $(\|\Delta(t)\|^2 + E_r^2(t))$  with and without adaptation of the synchronization gains. The non-adaptive case implements the controller (5) with  $\mu_{ij} = 0.2|\mathbf{q}_{ij}(0)|, \forall i = 1, \dots, 4, j \in N_i$ . Clearly, gain adaptation via (11) and (14) exhibits a significant improvement of the transient response over the non-adaptive case (5).

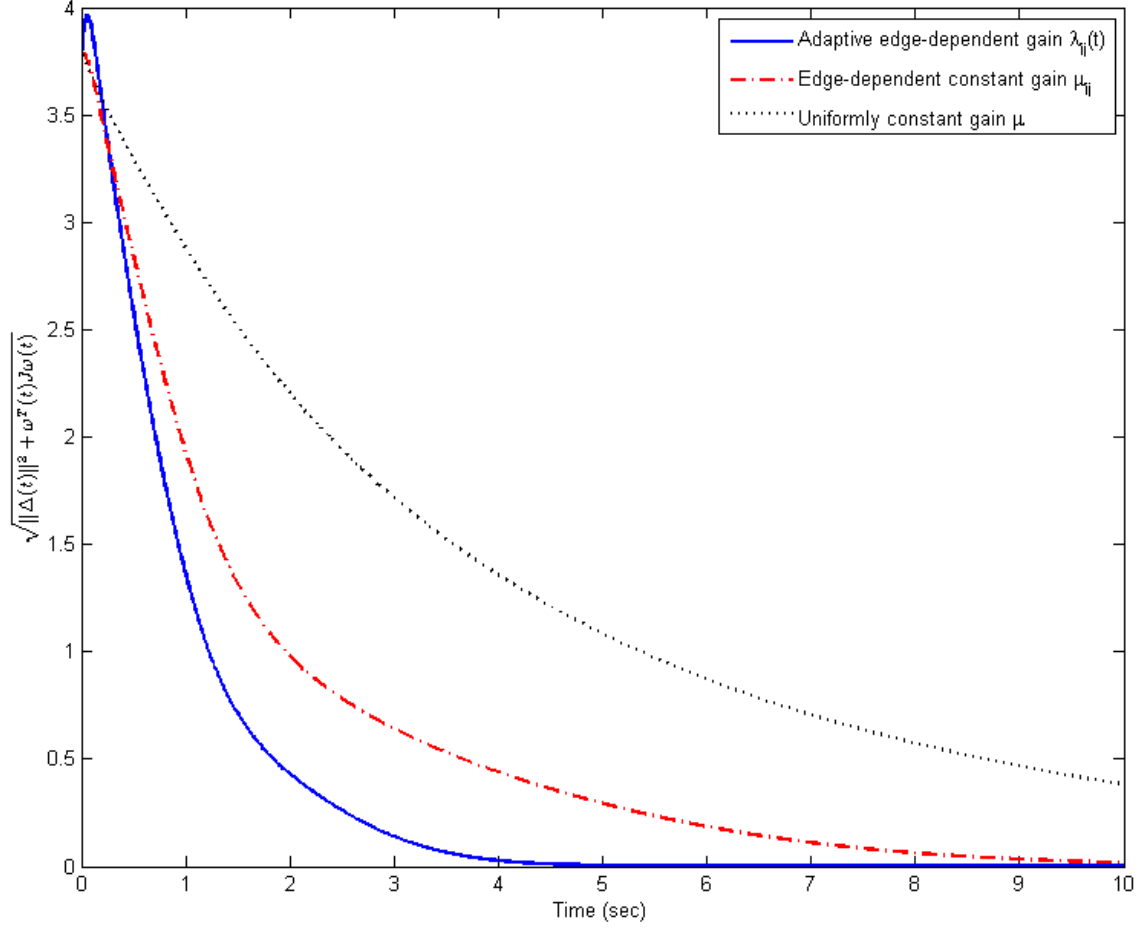


**Figure 10: Section 5.1.2 Evolution of  $\sqrt{\|\Delta(t)\|^2 + E_r^2(t)}$ .**

In order to optimize the adaptive synchronization gain, the effects of different gains  $\lambda_{ij}(t)$  in (11) (12) are examined. Choose  $\lambda_{ij}^*$  in terms of the initial mismatch of the spacecraft states as in (18), where  $\alpha \in [0.1, 2.1]$ . Figure 11 depicts both  $\|\Delta(t)\|$  and  $E_r(t)$  in terms of different  $\lambda_{ij}(t)$  to illustrate the selection of the optimal gain, which is  $\alpha = 0.6$ ,  $\lambda_{ij}^* = 0.6|\mathbf{q}_{ij}(0)|$ .

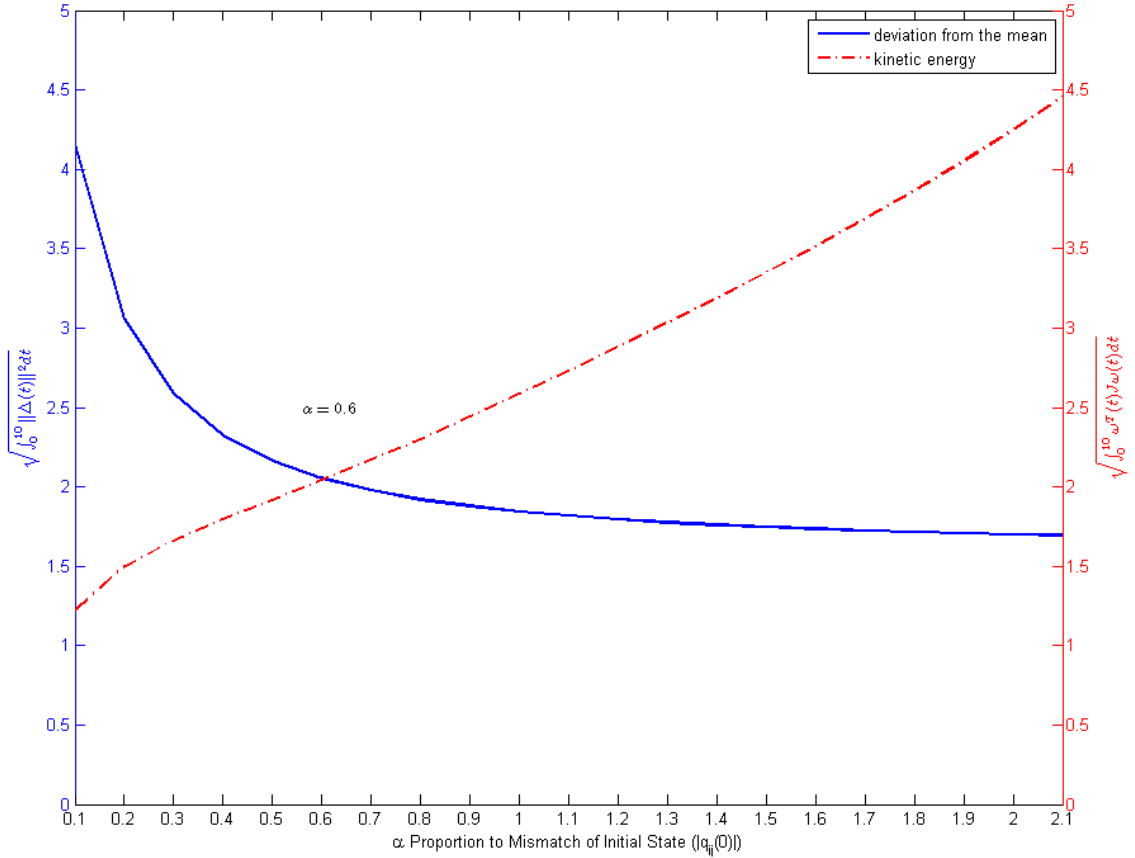


**Figure 11: Section 5.1.2 The effects of adaptive edge-dependent gain on  $\|\Delta(t)\|$  and  $E_r(t)$  in the range  $0.1 \leq \alpha \leq 2.1$ .**

## 5.2 Numerical study for the case of unknown parameters

To demonstrate the effectiveness of the proposed scheme in Chapter 4, consider a group of 4 spacecraft with a communication topology depicted in Figure 1. Use the same initial conditions as in Section 5.1. The true inertia matrices for each spacecraft are taken as

$$J_1 = \text{diag}(17,12,9), J_2 = \text{diag}(14,13,10),$$

$$J_3 = \text{diag}(20,10,9), J_4 = \text{diag}(15,9,16).$$

The actual external disturbances were chosen as

$$d_{ext,1} = 2.2, d_{ext,2} = 1.4, d_{ext,3} = 1.5, d_{ext,4} = 0.8.$$

A possible choice of the consensus gain for (15) is as in (26). Figure 12 and 13 show the attitude synchronization for regulation with  $\alpha = 0.2$  and  $\mathbf{\Gamma}_i = \text{diag}(3,3,3)$ . The results present the attitude error of spacecraft 2, 3 and 4 with respect to spacecraft 1, and the angular velocity of each spacecraft.

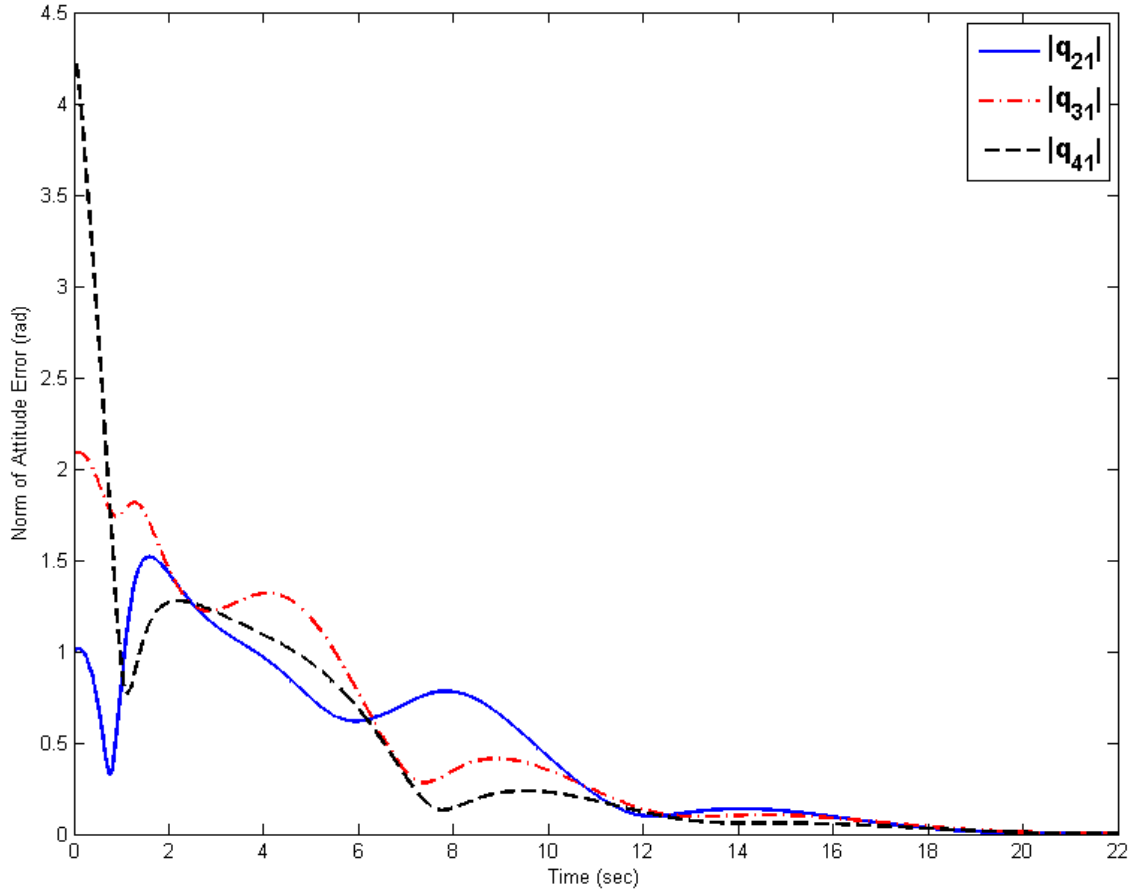


**Figure 12: Section 5.2 Evolution of attitude error with constant edge-dependent gain.**

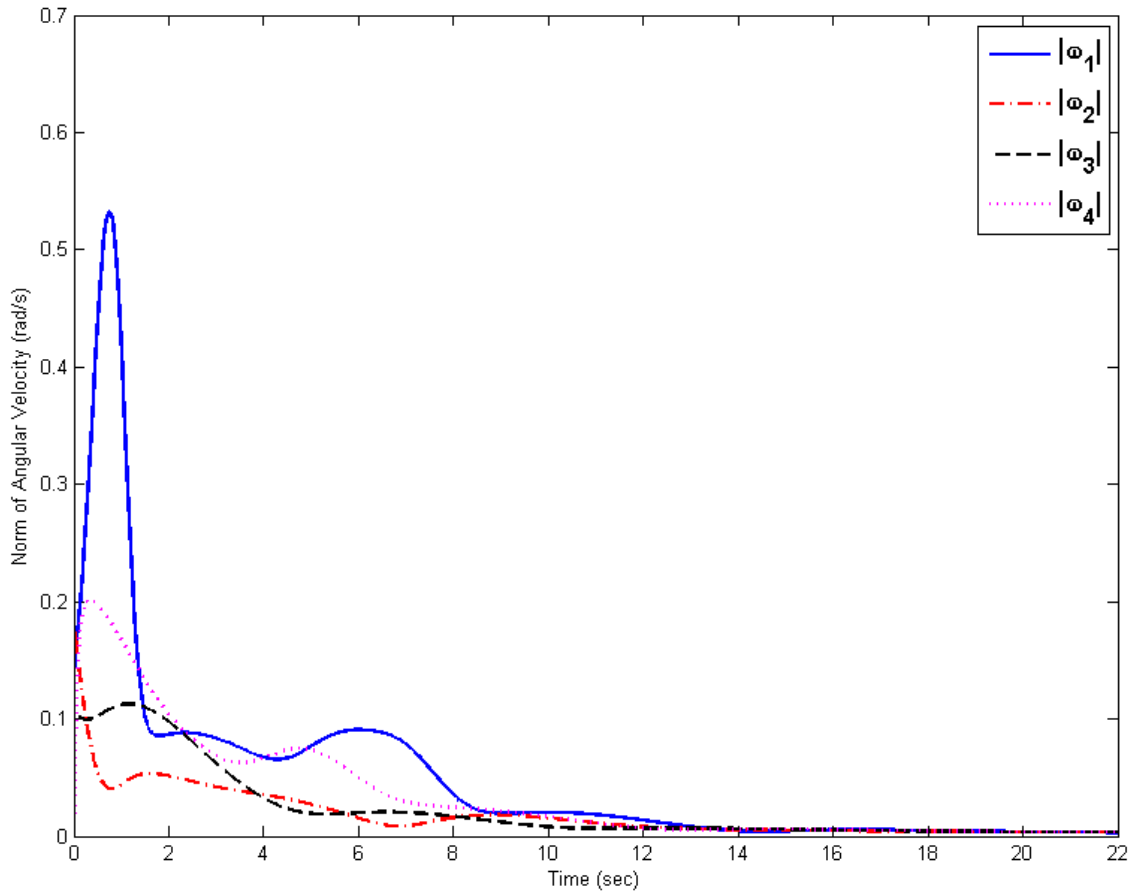


**Figure 13: Section 5.2 Evolution of angular velocity with constant edge-dependent gain.**

The choice of the optimal edge-dependent constant consensus gains satisfies equation (25). Examine the effect of different gains on  $\|\Delta(t)\|$  and  $E_r(t)$ . The result is presented in Figure14. It is observed that as the weight  $\alpha$  increases, which indicates the increase of  $\mu_{ij}$ , the deviation  $\Delta(t)$  decreases while the rotational kinetic energy  $E_r(t)$  increases. The intersection point at  $\alpha = 0.4078$  provides a good balance between the two performance metrics.

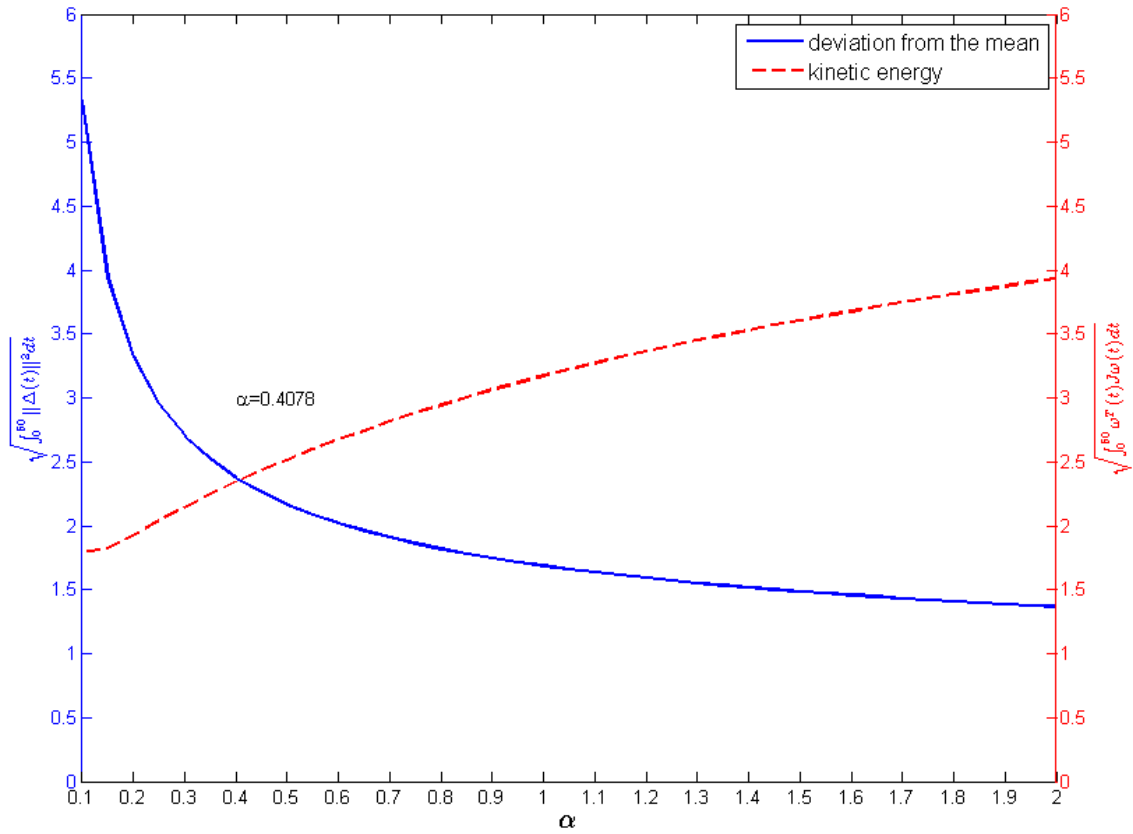


**Figure 14: Section 5.2 The effects of constant edge-dependent gain on  $\|\Delta(t)\|$  and  $E_r(t)$  in the range  $0.1 \leq \alpha \leq 2$ .**

For the proposed adaptive scheme (21) (23) (24), the attitude synchronization is tested with  $\lambda_{ij}^* = 0.4|\mathbf{q}_i(0) - \mathbf{q}_j(0)|$ ,  $\lambda_{ij}(t) = \lambda_{ij}^*$ ,  $\gamma_{ij} = 3$  and  $\mathbf{\Gamma}_i = \text{diag}(3,3,3)$ . The results are depicted in Figures 15 and 16. From these figures it can be observed that both the attitude synchronization and regulation objectives in (3) are met.

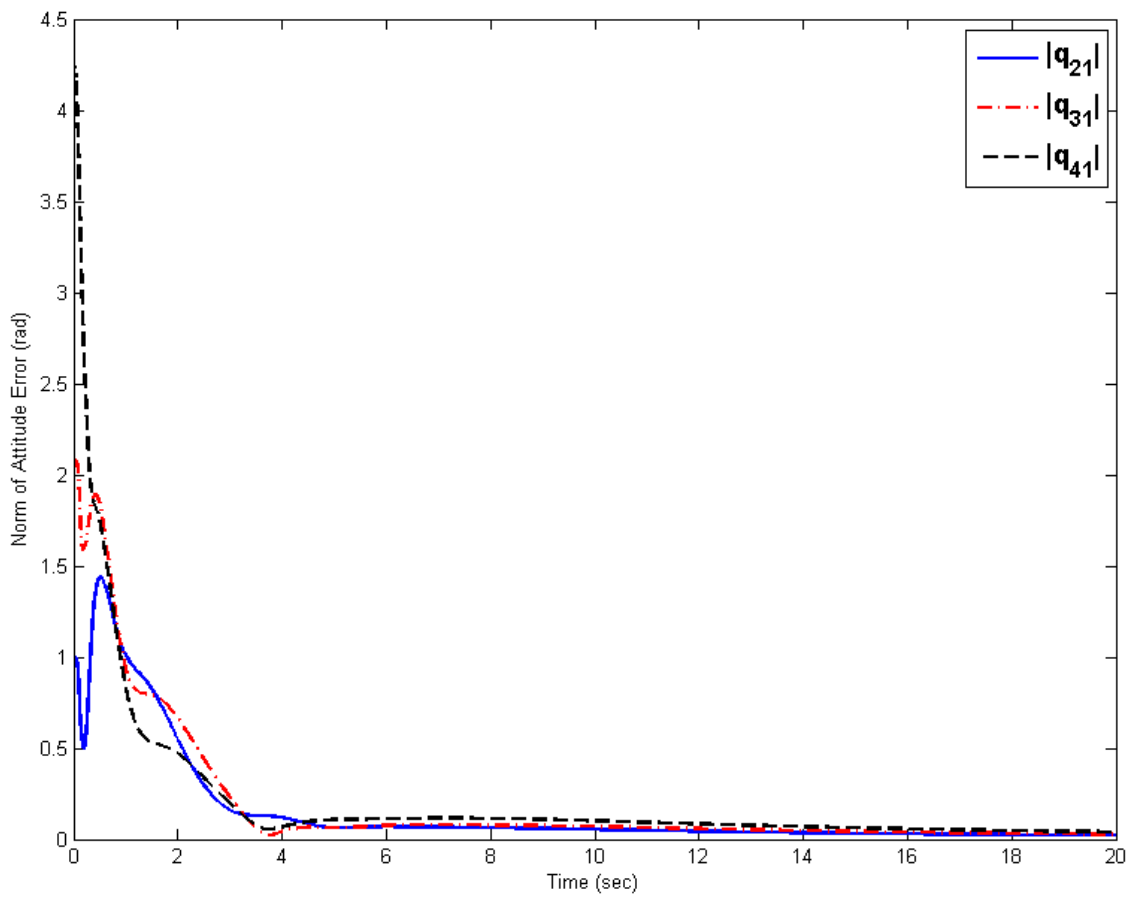


**Figure 15: Section 5.2 Evolution of attitude error with adaptive edge-dependent gain.**

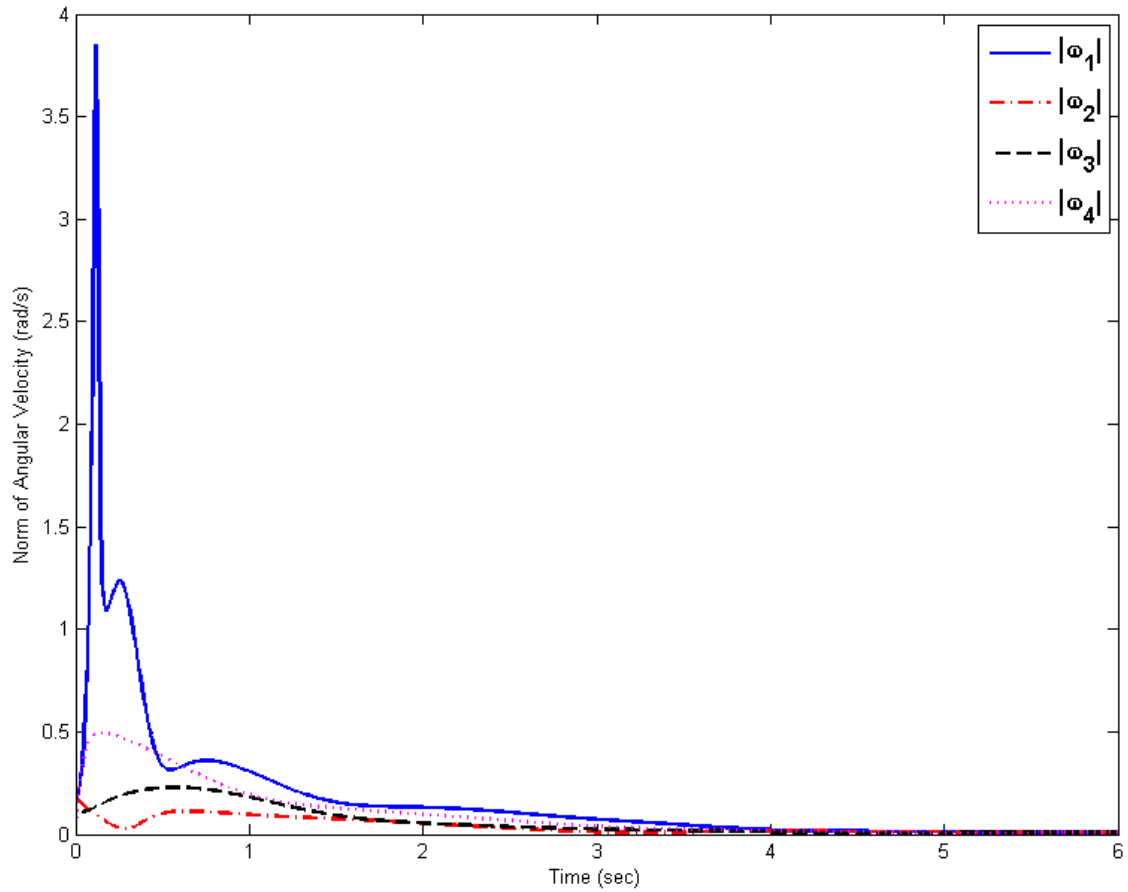
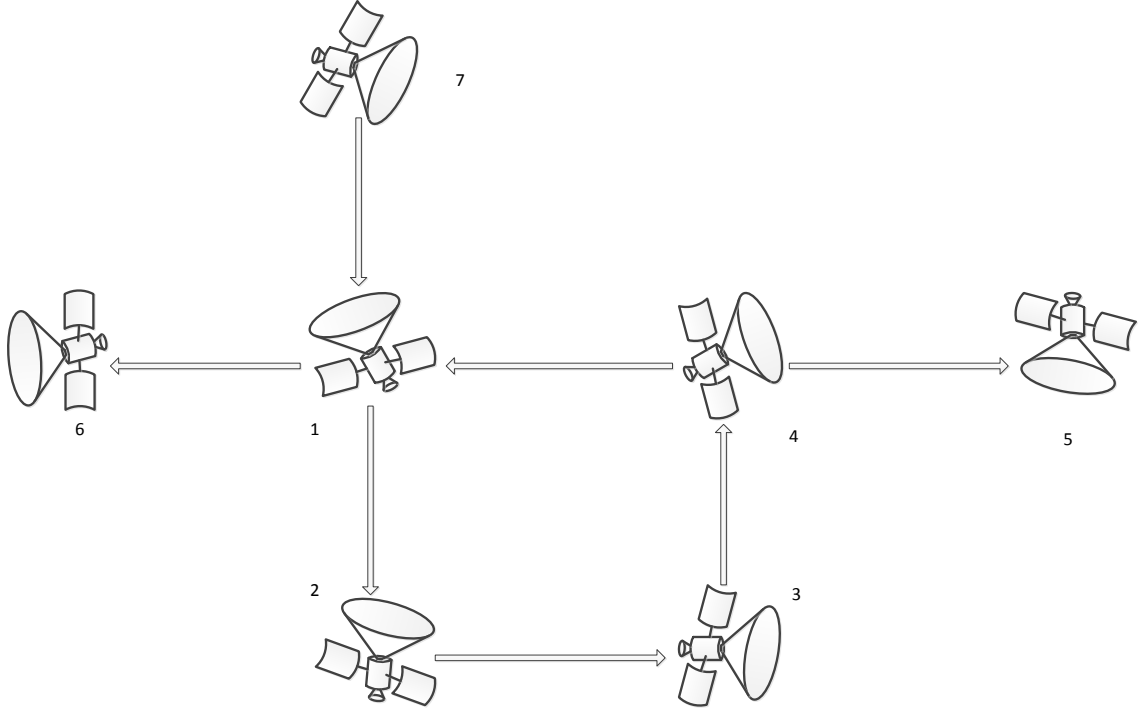


Figure 16: Section 5.2 Evolution of angular velocity with adaptive edge-dependent gain.

### 5.3 Example of more complex communication topology

#### 5.3.1 Communication topology with directed graph

Now consider a group of 7 spacecraft with a communication topology depicted in Figure17.



**Figure 17: Section 5.3.1 Directed graph on 7 spacecraft.**

The corresponding graph Laplacian matrix is given by

$$L(G) = \begin{bmatrix} 2 & 0 & 0 & -1 & 0 & 0 & -1 \\ -1 & 1 & 0 & 0 & 0 & 0 & 0 \\ 0 & -1 & 1 & 0 & 0 & 0 & 0 \\ 0 & 0 & -1 & 1 & 0 & 0 & 0 \\ 0 & 0 & 0 & -1 & 1 & 0 & 0 \\ -1 & 0 & 0 & 0 & 0 & 1 & 0 \\ 0 & 0 & 0 & 0 & 0 & 0 & 0 \end{bmatrix}$$

The initial conditions of these 7 spacecraft are

$$\begin{aligned} \mathbf{q}_1(0) &= [3.0 \quad 2.0 \quad 1.0]^T, \mathbf{q}_2(0) = [3.2 \quad 2.4 \quad 1.9]^T, \mathbf{q}_3(0) = [2.7 \quad 1.2 \quad 2.9]^T, \\ \mathbf{q}_4(0) &= [3.1 \quad 2.2 \quad 2.0]^T, \mathbf{q}_5(0) = [2.5 \quad 3.0 \quad 2.3]^T, \mathbf{q}_6(0) = [3.5 \quad 2.4 \quad 1.6]^T, \\ \mathbf{q}_7(0) &= [2.8 \quad 1.6 \quad 2.5]^T. \end{aligned}$$

and the inertia matrices of each spacecraft are chosen as

$$\begin{aligned} J_1 &= \text{diag}(17,12,9), J_2 = \text{diag}(14,13,10), J_3 = \text{diag}(20,10,9), J_4 = \text{diag}(15,9,16), \\ J_5 &= \text{diag}(10,15,12), J_6 = \text{diag}(16,14,8), J_7 = \text{diag}(14,17,10). \end{aligned}$$

Simulation regarding the regulation case is implemented.

Similarly, test the attitude synchronization with  $\alpha = 1.0$ ,  $\mu_{ij} = |\mathbf{q}_i(0) - \mathbf{q}_j(0)|$ ,  $i = 1, \dots, N, j \in N_i$ . The results are depicted in Figure 18 and 19. It can be observed that both the attitude synchronization and regulation objectives in (3) are achieved.

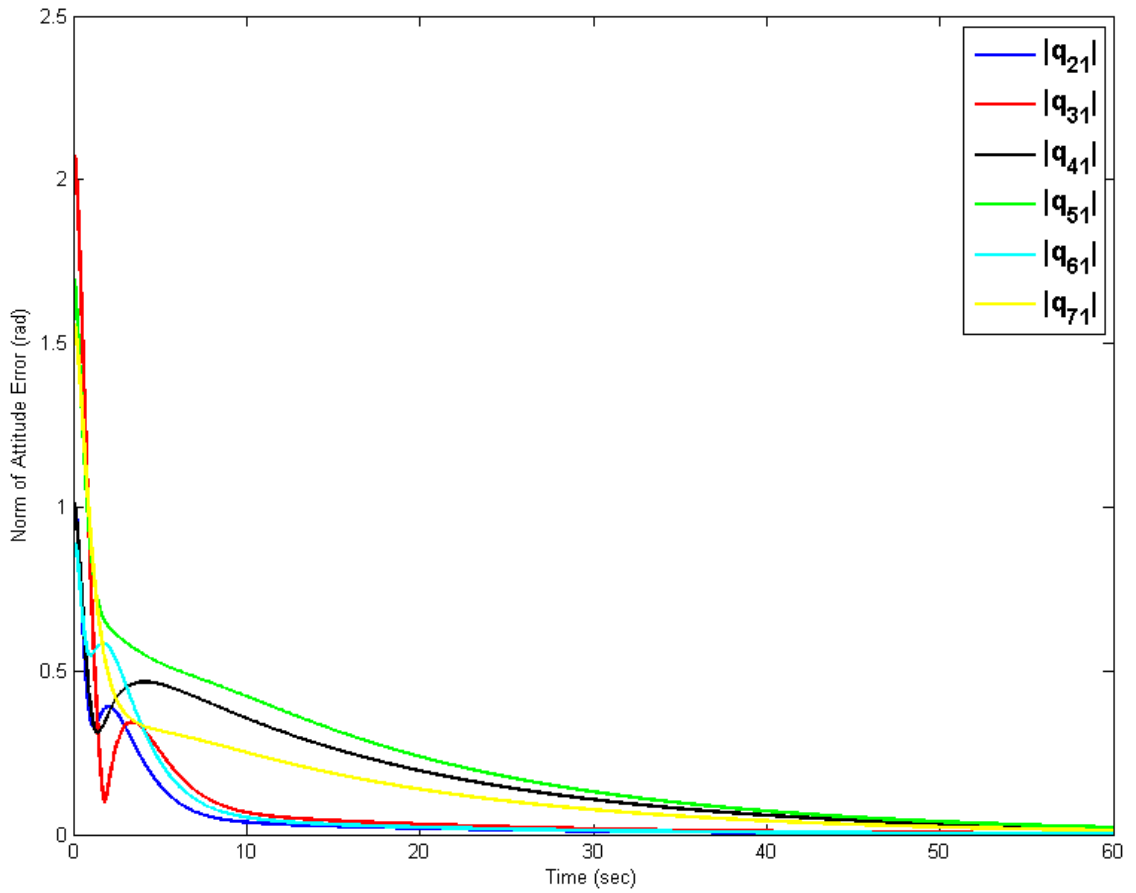


**Figure 18: Section 5.3.1 Evolution of attitude error with constant edge-dependent gain.**

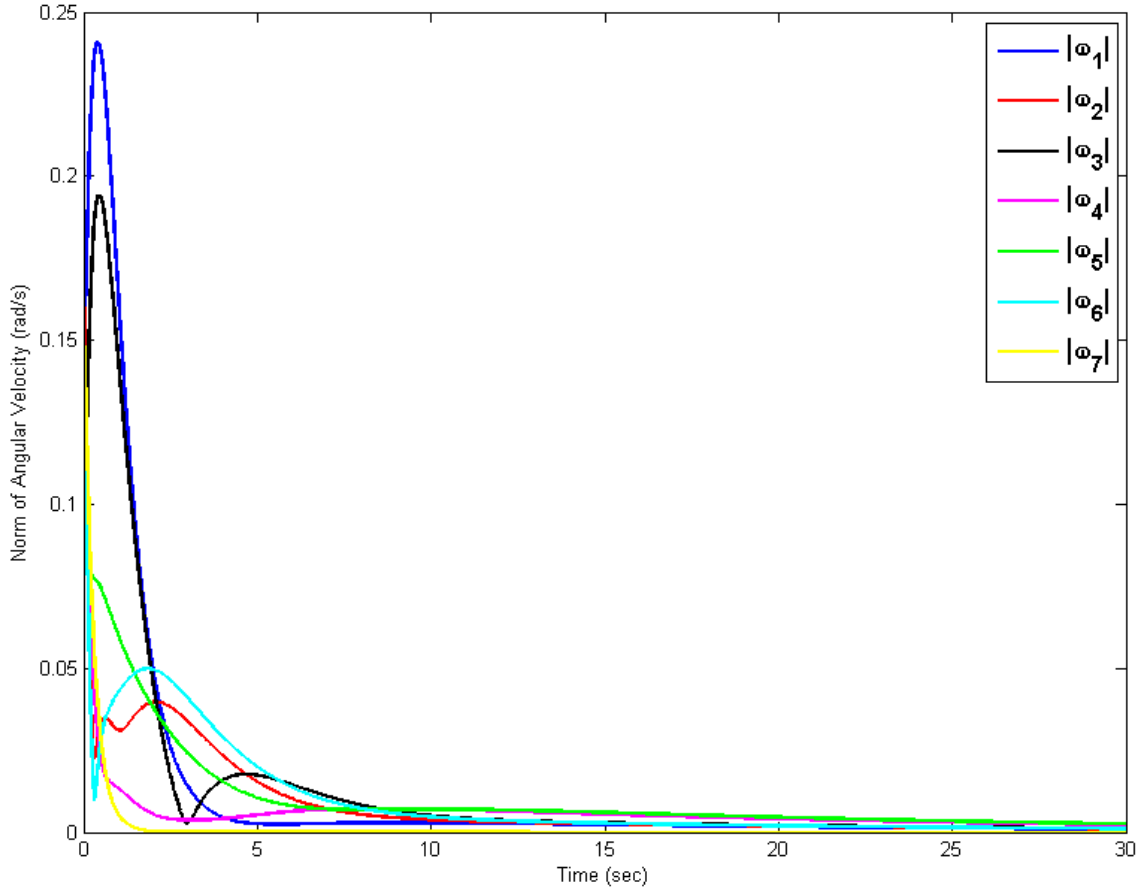


**Figure 19: Section 5.3.1 Evolution of angular velocity with constant edge-dependent gain.**

Besides, different values of the uniform gain  $\mu$  in the range  $0.5 \leq \mu \leq 6$  were considered, see Figure 20. The closed-loop systems (6) were simulated over the time interval  $[0,30]$ s. Both  $L_2(0,30; \mathbb{R}^{3N})$  norm of  $\Delta(t)$  and  $L_2(0,30; \mathbb{R}^1)$  norm of  $E_r(t)$  were calculated for each  $\mu \in [0.5,6]$ . An optimal value of the synchronization gain  $\mu$  locates at the intersection point  $\mu = 1.65$  provides good balance between these two performance metrics.

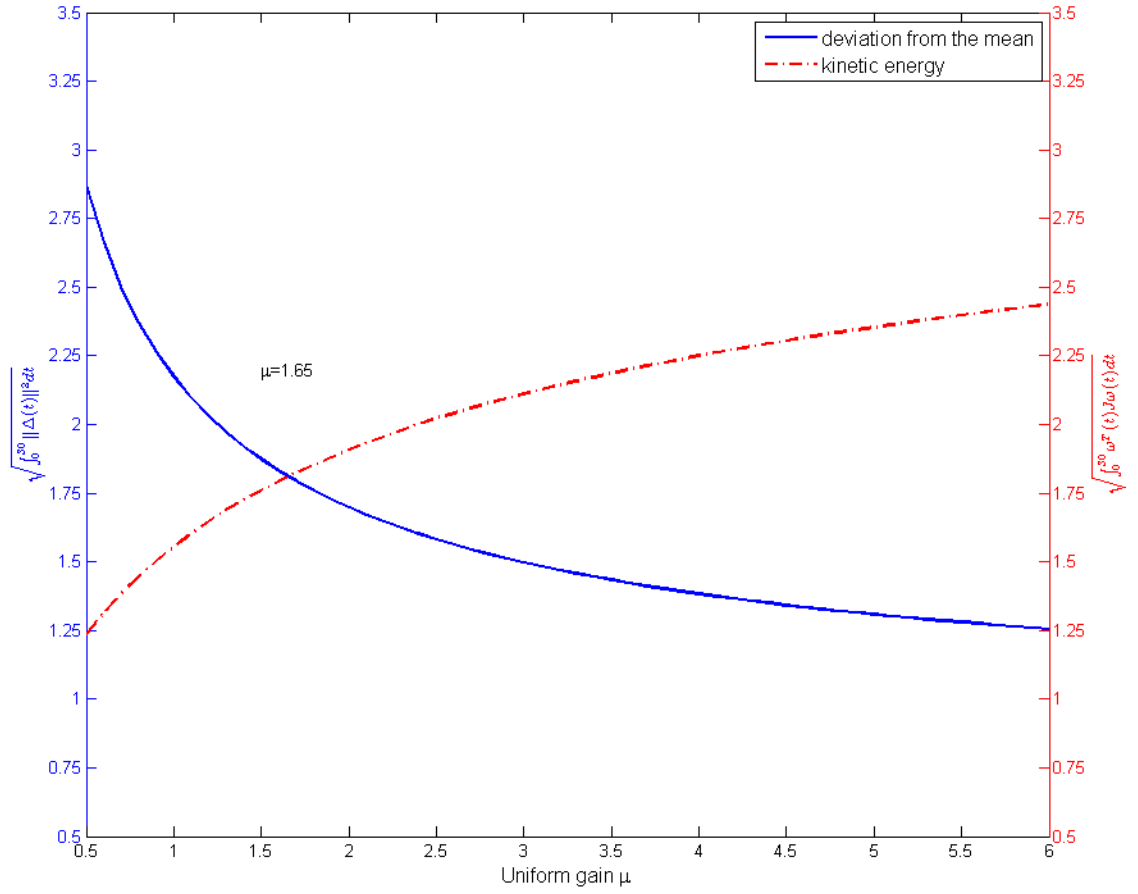


**Figure 20: Section 5.3.1 The effects of varying the uniform fixed gain in the range  $0.5 \leq \mu \leq 6$  on  $\|\Delta(t)\|$  and  $E_r(t)$ .**

Now optimize the adaptive synchronization gains  $\lambda_{ij}(t)$  in (11) (12). Choose  $\lambda_{ij}^*$  in terms of the initial mismatch of the spacecraft states as in (18), where  $\alpha \in [0.5, 6]$ . Both  $\|\Delta(t)\|$  and  $E_r(t)$  in terms of different  $\lambda_{ij}(t)$  to are depicted Figure 21, from which the best selection of the optimal gain is  $\alpha = 1.97$ ,  $\lambda_{ij}(0) = \lambda_{ij}^* = 1.97|\mathbf{q}_{ij}(0)|$ .

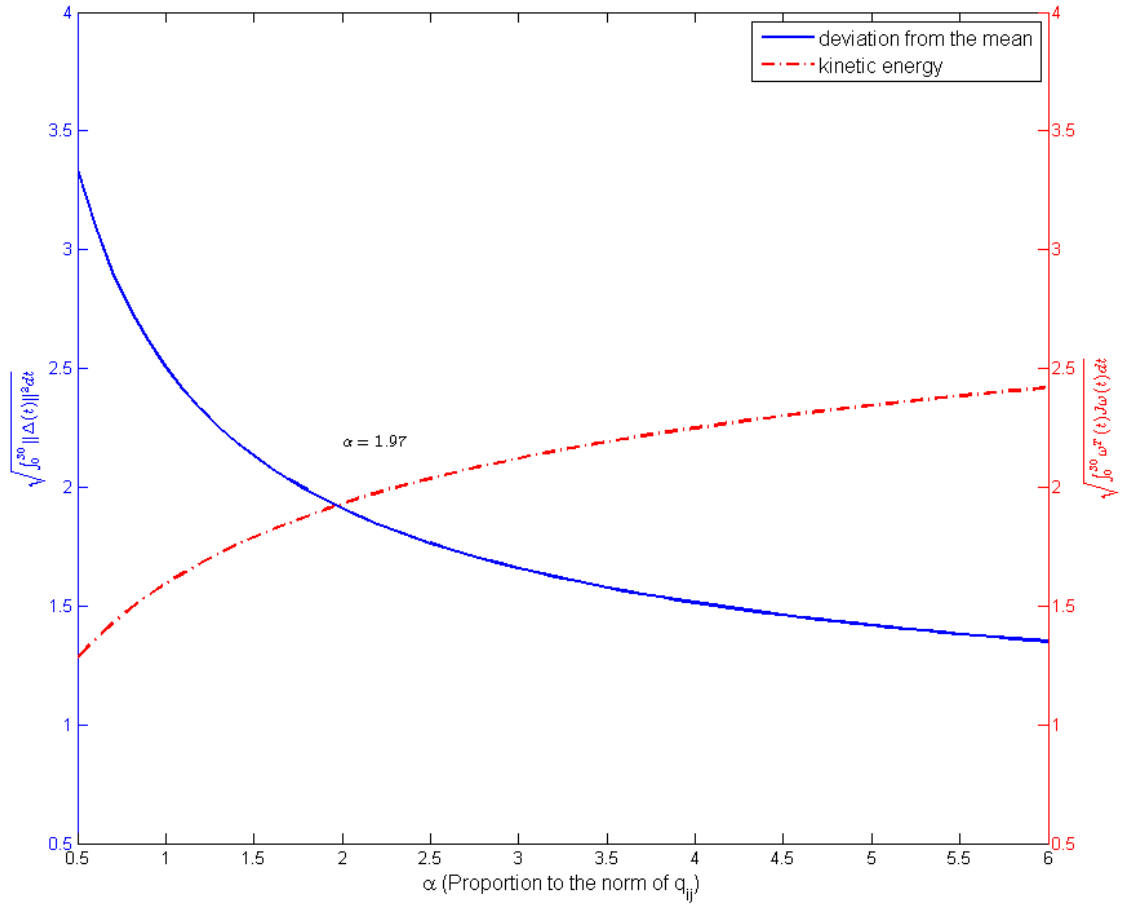


**Figure 21: Section 5.3.1 The effects of adaptive edge-dependent gain on  $\|\Delta(t)\|$  and  $E_r(t)$  in the range  $0.5 \leq \alpha \leq 6$ .**

### 5.3.2 Communication topology with undirected graph

The above simulations all use topology with directed graph. Now, numerical study is done to demonstrate that our theoretical results are also suitable for undirected graph (see in Figure 22).

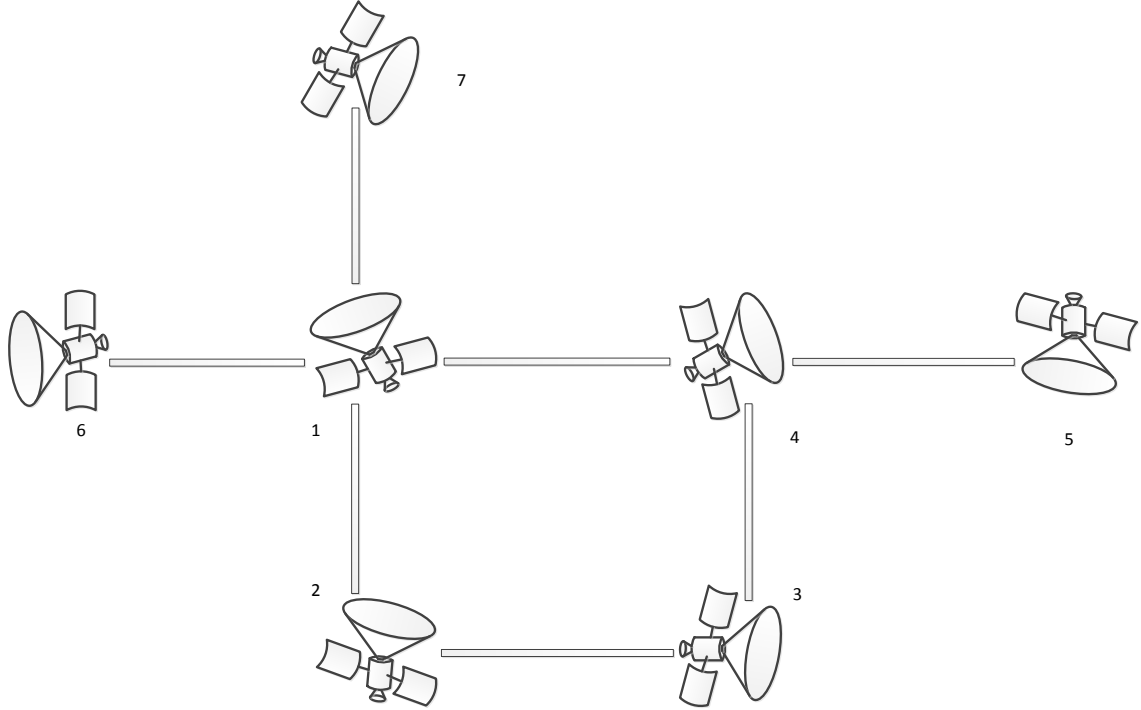


**Figure 22: Section 5.3.2 Undirected graph on 7 spacecraft.**

The corresponding graph Laplacian matrix is given by

$$L(G) = \begin{bmatrix} 4 & -1 & 0 & -1 & 0 & -1 & -1 \\ -1 & 2 & -1 & 0 & 0 & 0 & 0 \\ 0 & -1 & 2 & -1 & 0 & 0 & 0 \\ -1 & 0 & -1 & 3 & -1 & 0 & 0 \\ 0 & 0 & 0 & -1 & 1 & 0 & 0 \\ -1 & 0 & 0 & 0 & 0 & 1 & 0 \\ -1 & 0 & 0 & 0 & 0 & 0 & 1 \end{bmatrix}$$

Use the same initial condition and inertia moment as section 5.3.1.

Study the attitude synchronization with  $\alpha = 0.5$  in (26). With control law (5) and 6, the results are depicted in Figures 23 and 24. It can be observed that both the attitude synchronization and regulation objectives in (3) are achieved.

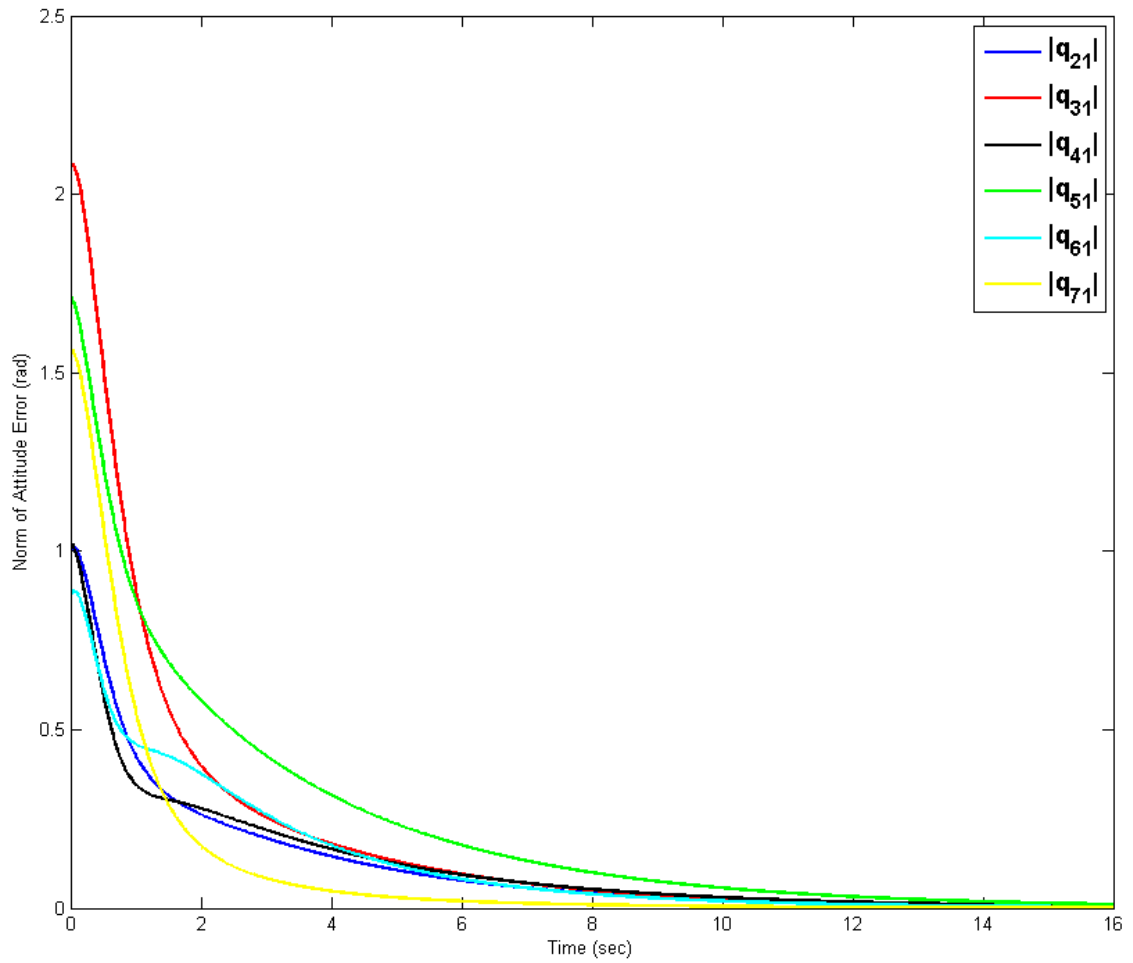


**Figure 23: Section 5.3.2 Evolution of attitude error with constant edge-dependent gain.**

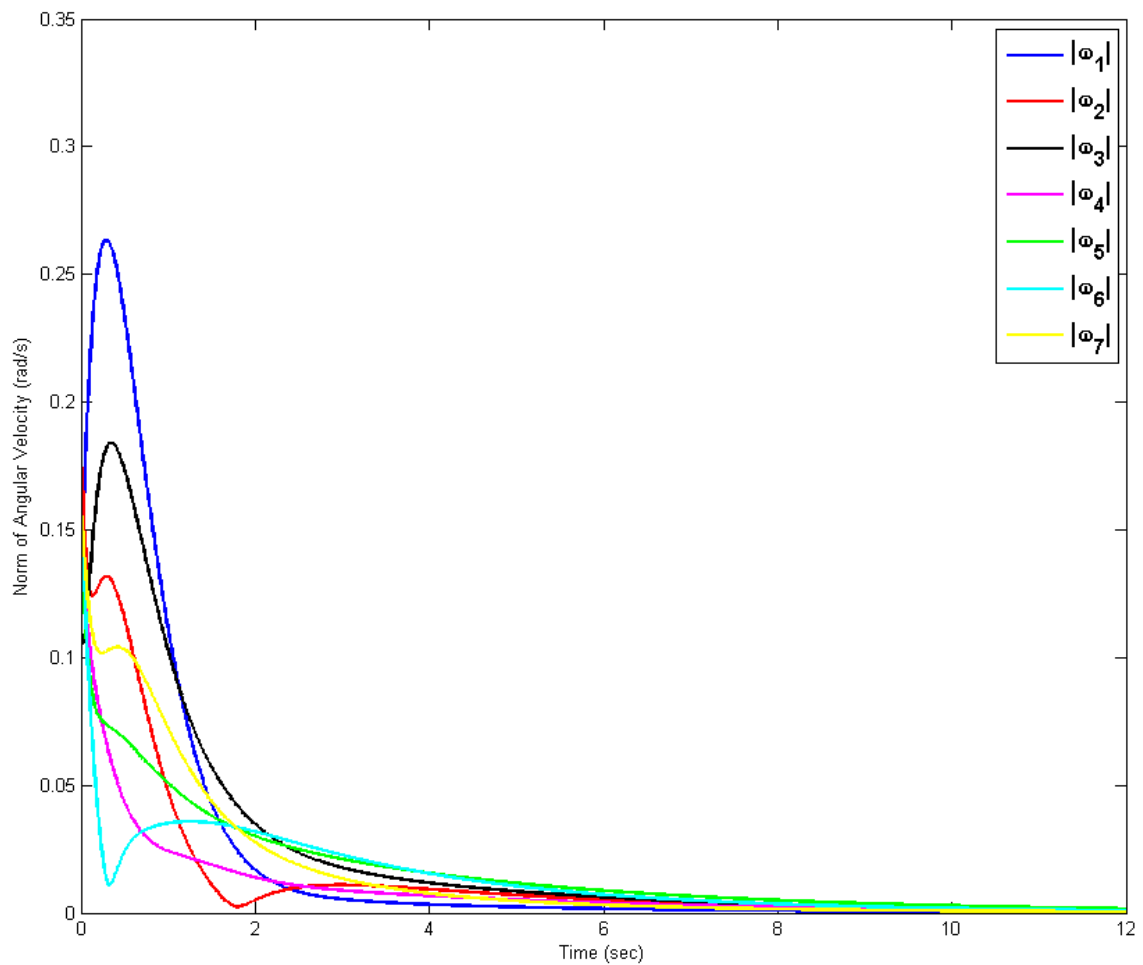


**Figure 24: Section 5.3.2 Evolution of angular velocity with constant edge-dependent gain.**

First, test the effects of different uniform gains  $\mu \in [0.1,6]$ . From Figure 25, it can be seen that the best selection of the optimal gain is  $\mu = 1.44$ .

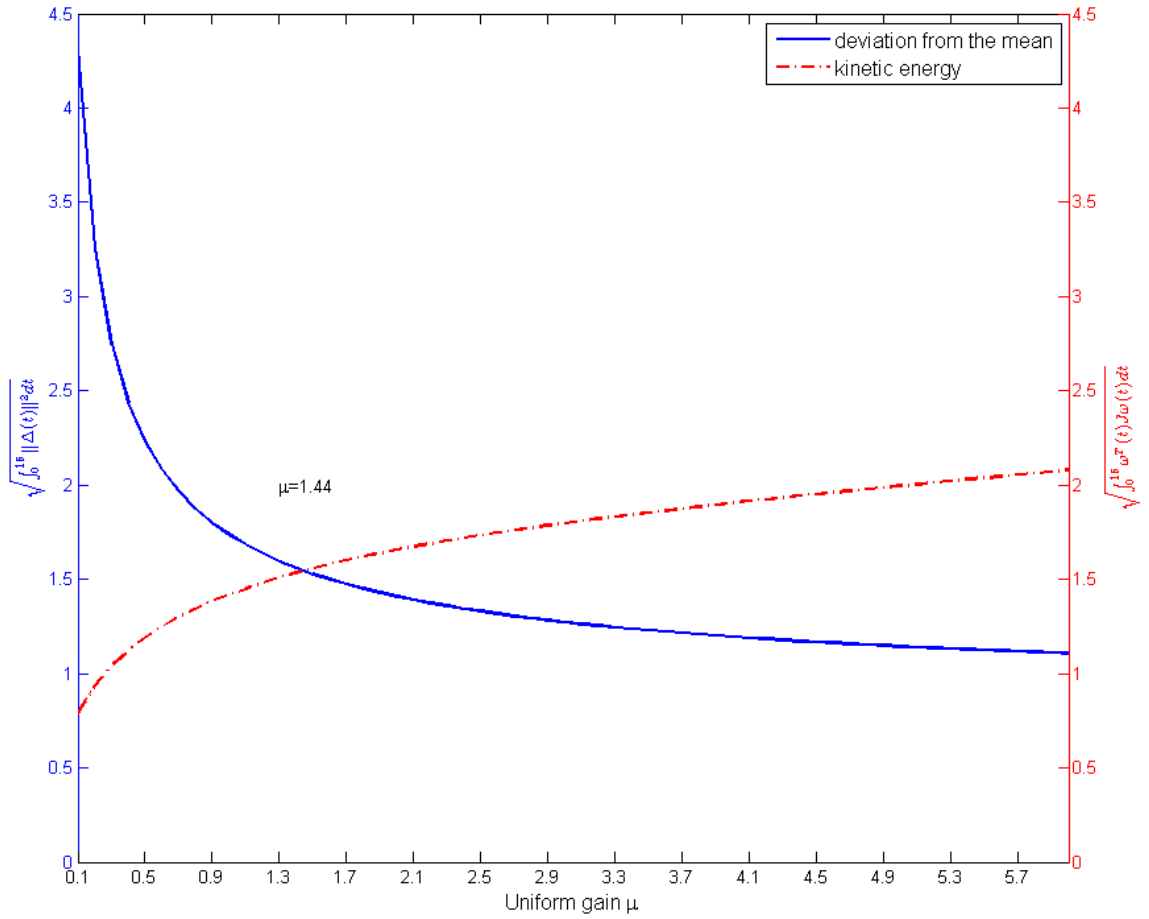


**Figure 25: Section 5.3.2 The effects of varying the uniform fixed gain on the range  $0.1 \leq \mu \leq 6$  on  $\|\Delta(t)\|$  and  $E_r(t)$ .**

Then, examine the effects of different gains  $\mu_{ij}$  in (4) and (5) to choose the optimal synchronization gains in terms of the initial mismatch of the spacecraft states as (26).

One can find that when  $\alpha = 1.48$  in (26), the result is best.

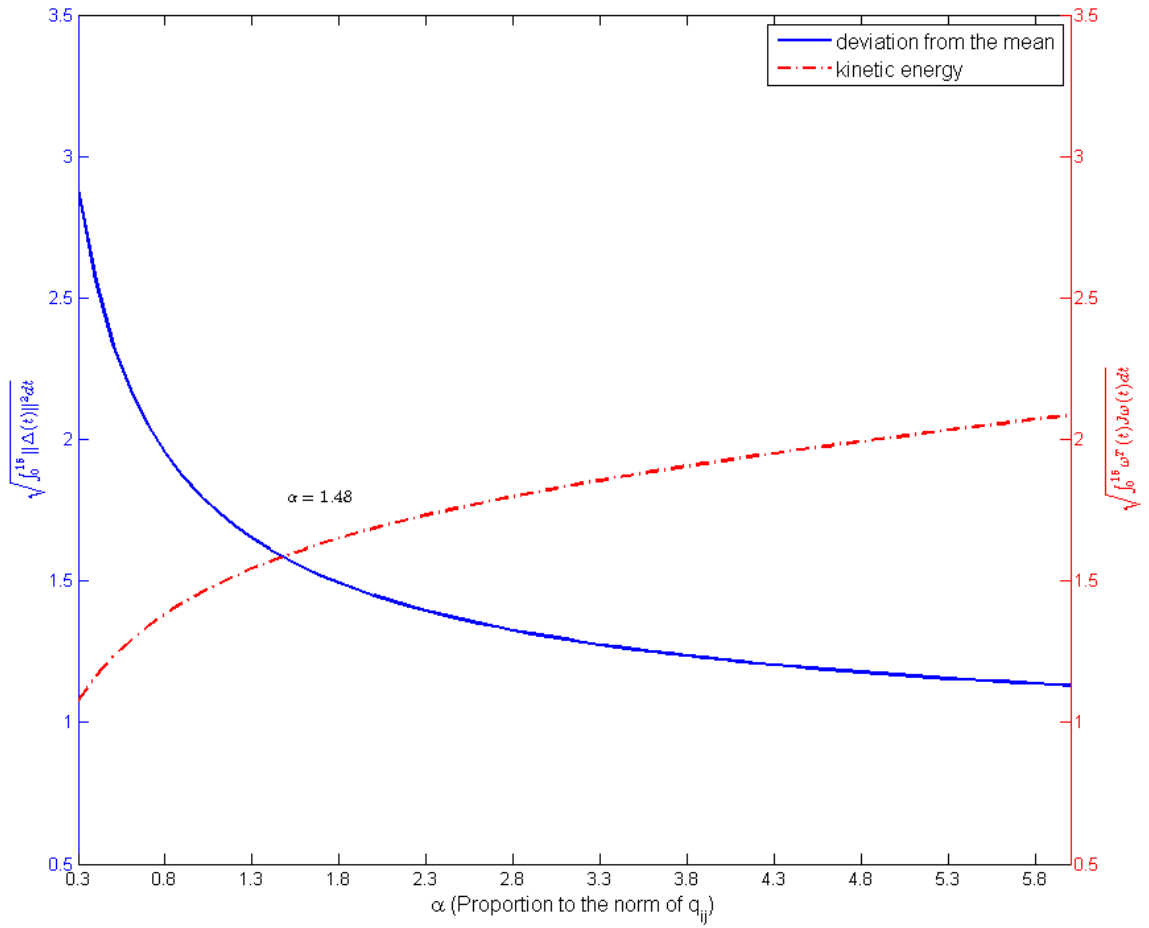


**Figure 26: Section 5.3.2 The effects of edge-dependent gain on  $\|\Delta(t)\|$  and  $E_r(t)$  in the range  $0.3 \leq \alpha \leq 6$ .**

#### 5.4 Specific study on the effect of adaptation of synchronization gains

In order to have a more comprehensive understanding about the effect of edge-dependent adaptive synchronization gains, use a simple topology of 2 spacecraft shown in Figure 27.



**Figure 27: Section 5.4 Communication topology with 2 spacecraft.**

The corresponding Laplacian matrix of the above graph is

$$L(G) = \begin{bmatrix} 1 & -1 \\ -1 & 1 \end{bmatrix}$$

with initial condition  $\mathbf{q}_1(0) = [3.0 \ 2.0 \ 1.0]^T$ ,  $\mathbf{q}_2(0) = [3.2 \ 2.4 \ 1.9]^T$  and the inertia matrices  $J_1 = \text{diag}(17,12,9)$ ,  $J_2 = \text{diag}(14,13,10)$ .

Choose  $\lambda_{12}(0) = \lambda_{12}^* = \alpha_{12} * |\mathbf{q}_1(0) - \mathbf{q}_2(0)|$  and  $\lambda_{21}(0) = \lambda_{21}^* = \alpha_{21} * |\mathbf{q}_2(0) - \mathbf{q}_1(0)|$  in (10) (11) and (12), where  $0.1 \leq \alpha_{12} \leq 4.0$  and  $0.1 \leq \alpha_{21} \leq 4.0$ .

Figure 28 clearly shows the effect of different pair of  $\lambda_{12}^*$  and  $\lambda_{21}^*$  on  $\|\Delta(t)\|$  and  $E_r(t)$ . It can be seen that  $\lambda_{12}^*$  and  $\lambda_{21}^*$  locating on the curve highlighted by red give out optimal synchronization gains for the adaptive case.

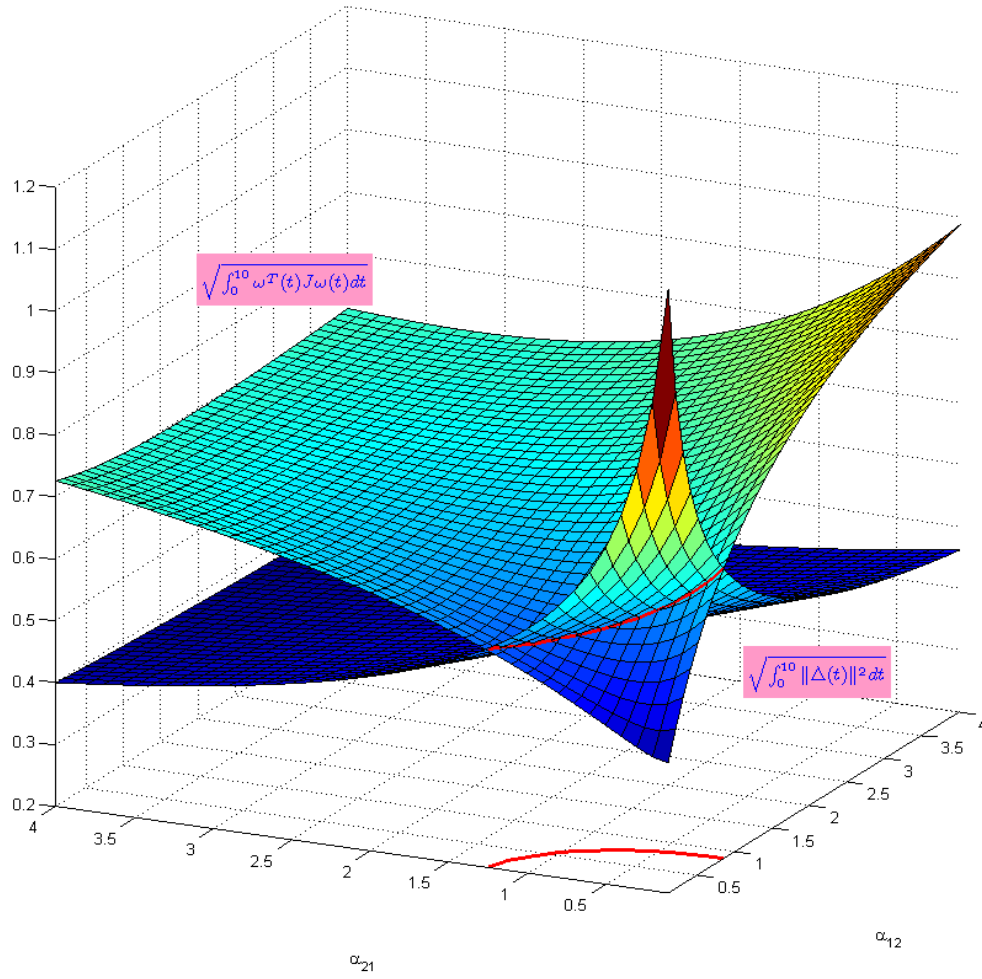


**Figure 28: Section 5.4 The effects of adaptive edge-dependent gain on  $\|\Delta(t)\|$  and  $E_r(t)$  with different  $\lambda_{12}^*$  and  $\lambda_{21}^*$ .**

In order to show the improvement of the optimal synchronization gains over the gains that are chosen from other values, compare the  $L_2(0,10)$  norm of  $(\|\Delta(t)\|^2 + E_r^2(t))$  presented in Table 1. One can find that the optimal gain gives out a better result.

**Table 1:**  $L_2(\mathbf{0}, \mathbf{10})$  norm of  $(\|\Delta(t)\|^2 + E_r^2(t))$ 

Case $(\lambda_{12}^* = \alpha_{12} \mathbf{q}_{12}(0) , \lambda_{21}^* = \alpha_{21} \mathbf{q}_{21}(0) $ in (10) and (11))	$L_2(\mathbf{0}, \mathbf{10})$ norm of $(\ \Delta(t)\ ^2 + E_r^2(t))$
$\alpha_{12} = 0.2 ; \alpha_{21} = 0.2$	0.993345
$\alpha_{12} = 0.3 ; \alpha_{21} = 0.8$ (chosen from the highlighted curve in Figure 28)	0.788357
$\alpha_{12} = 3.8 ; \alpha_{21} = 0.5$	0.998867

# Chapter 6

## Conclusion and Future Work

### 6.1 Conclusion

This thesis considered the optimization aspects of the control problem of attitude synchronization of spacecraft formation with both known and unknown parameters and external disturbances. In particular two modifications in consensus penalty terms were proposed. First, node-independent constant synchronization gains chosen by penalizing the difference between the initial states of spacecraft were examined to prove their superiority over arbitrary ones. A performance-based optimization was also proposed for edge-dependent synchronization gains that minimized a combination of the rotational kinetic energy (stability) and the deviation-from-the-mean (synchronization performance). Subsequently, an adaptation of the consensus gains was presented and which resulted in a significant improvement of the transient response. Such an adaptation utilized Lyapunov-redesign methods to extract adaptation laws for the synchronization gain updates that were expressed in terms of

the pairwise differences of spacecraft states. Extensive simulation studies were included in order to further support the theoretical predictions.

## **6.2 Future work**

The research work here was conducted under the assumption that knowledge of the attitude and angular velocity of each spacecraft and its neighbors were available. This full-state knowledge paves the way for a base line comparison when partial state information combined with time delays are considered.

The future research will expand the adaptive attitude synchronization of spacecraft formation to the cases of leader-follower and possible time-delay. Associated with these two cases are the mechanisms in obtaining attitude states and signals from neighbors.

In the leader-follower case, a given spacecraft should track the trajectory of the “leader”, which requires each spacecraft access the reference trajectory directly or indirectly. The distributed attitude synchronization and tracking should still be achieved through the appropriate control input.

In general, the communication among the spacecraft has certain delays due to distance and disturbance. Therefore, it is more realistic to consider time delays when dealing with attitude synchronization. This is a more complicated situation which will be examined in the future.

# References

- [1] Sun, D., Synchronization and control of multiagent systems, CRC Press LLC, 2010.
- [2] Scharf, D. P., Hadaegh, F. Y., and Ploen, S. R., “A survey of spacecraft formation flying guidance and control (part I): Guidance,” Proceedings of the American control conference, Vol. 2, American Automatic Control Council, 2003, pp. 1733-1739.
- [3] Scharf, D. P., Hadaegh, F. Y., and Ploen, S. R., “A survey of spacecraft formation flying guidance and control (part II): Control,” American Control Conference, 2004. Proceedings of the 2004, Vol. 4, IEEE, 2004, pp. 2976-2985.
- [4] De Lellis, P., Di Bernardo, M., Sorrentino, F., and Tierno, A., “Adaptive synchronization of complex networks,” International Journal of Computer Mathematics, Vol. 85, No. 8, 2008, pp. 1189-1218.
- [5] De Lellis, P., Di Bernardo, M., and Garofalo, F., “Vertex-based adaptive synchronization of complex networks,” Circuits and Systems, 2008. ISCAS 2008. IEEE International Symposium on, IEEE, 2008, pp. 2526-2529.
- [6] De Lellis, P. and Di Bernardo, M., “Robustness of local adaptive synchronization strategies to topological variations and delays,” Circuits and Systems, 2009. ISCAS 2009. IEEE International Symposium on, IEEE, 2009, pp. 1609-1612.
- [7] Igarashi, Y., Hatanaka, T., Fujita, M., and Spong, M. W., “Passivity-based attitude synchronization in  $SE(3)$ ,” Control Systems Technology, IEEE Transactions on, Vol. 17, No. 5, 2009, pp. 1119-1134.

- [8] Lee, U. and Mesbahi, M., "Spacecraft synchronization in the presence of attitude constrained zones," American Control Conference (ACC), 2012, IEEE, 2012, pp. 6071-6076.
- [9] Min, H., Wang, S., Sun, F., Gao, Z., and Zhang, J., "Decentralized adaptive attitude synchronization of spacecraft formation," Systems & Control Letters, Vol. 61, No. 1, 2012, pp. 238-246.
- [10] Zhou, J., Ma, G., and Hu, Q., "Delay depending decentralized adaptive attitude synchronization tracking control of spacecraft formation," Chinese Journal of Aeronautics, Vol. 25, No. 3, 2012, pp. 406-415.
- [11] Nuño, E., Ortega, R., and Basañez, L., "An adaptive controller for nonlinear teleoperators," Automatica, Vol. 46, No. 1, 2010, pp. 155-159.
- [12] Chopra, N., Spong, M. W., and Lozano, R., "Synchronization of bilateral teleoperators with time delay," Automatica, Vol. 44, No. 8, 2008, pp. 2142-2148.
- [13] Siciliano, B. and Khatib, O., Springer handbook of robotics, Springer, 2008.
- [14] Chung, S. J., Ahsun, U., and Slotine, J. J. E., "Application of synchronization to formation flying spacecraft: Lagrangian approach," Journal of Guidance, Control, and Dynamics, Vol. 32, No. 2, 2009, pp. 512-426.
- [15] Kuipers, J. B., Quaternions and rotation sequences: a primer with applications to orbits, aerospace, and virtual reality, Princeton university press, 1999.
- [16] Shuster, M. D., "A survey of attitude representations," The Journal of the Astronautical Sciences, Vol. 41(4), pp. 439-517, 1993.
- [17] Shuster, M. D., "The nature of the quaternion," The Journal of the Astronautical Sciences, Vol. 56(3), pp. 359-373, 2008.

- [18] Wie, B., Space vehicle dynamics and control, AIAA, 1998.
- [19] Lewis, F. L., Dawson, D. M., and Abdallah, C. T., Robot manipulator control: theory and practice, Vol. 15, CRC Press, 2003.
- [20] Kelly, R., Santibáñez, V., Davila, V. S., and Loría, A., Control of robot manipulators in joint space, Springer, 2005.
- [21] Spong, M. W., Hutchinson, S., and Vidyasagar, M., Robot modeling and control, John Wiley & Sons New York, 2006.
- [22] Mesbahi, M. and Egerstedt, M., Graph theoretic methods in multiagent networks, Princeton University Press, 2010.
- [23] Diestel, R., Graph theory, Springer, 2005.
- [24] Slotine, J. -J. E. and Li, W., Applied nonlinear control, Prentice Hall New Jersey, 1991.
- [25] Zhang, K. and Demetriou, M. A., “Attitude synchronization of spacecraft formation with adaptation of consensus penalty terms,” Proceedings of the European Control Conference, July 2003.
- [26] Haddad, W. M. and Chellaboina, V., Nonlinear dynamical systems and control: a Lyapunov-based approach, Princeton University Press, 2011.
- [27] Ren, W., Beard, R. W., and McLain, T. W., “Coordination variables and consensus building in multiple vehicle systems,” Cooperative Control, Springer, 2005, pp. 171-188.
- [28] Ioannou, P. A. and Sun, J., Robust adaptive control, Courier Dover Publications, 2012.